Optical and microphysical properties of natural mineral dust and anthropogenic soil dust near dust source regions over northwestern China

Xin Wang[1], Hui Wen[1], Jinsen Shi[1], Jianrong Bi[1], Zhongwei Huang[1], Beidou Zhang[1], Tian Zhou[1], Kaiqi Fu[1], Quanliang Chen[2], and Jinyuan Xin[3]

[1] Key Laboratory for Semi-Arid Climate Change of the Ministry of Education, College of Atmospheric Sciences, Lanzhou University, Lanzhou 730000, China

[2] Plateau Atmospheric and Environment Laboratory of Sichuan Province, College of Atmospheric Sciences, Chengdu University of Information Technology, Chengdu 610225, China

[3] State Key Laboratory of Atmospheric Boundary Layer Physics and Atmospheric Chemistry (LAPC), Institute of Atmospheric Physics, Chinese Academy of Sciences, Beijing 100029, China

Correspondence to: X. Wang (wxin@lzu.edu.cn)

Abstract.

Mineral dust aerosols (MDs) not only influence the climate by scattering and absorbing solar radiation, but also modify cloud properties and change the ecosystem. From 3 April to 16 May 2014, a ground-based mobile laboratory was deployed to measure the optical and microphysical properties of MDs near dust source regions in Wuwei, Zhangye, and Dunhuang (in chronological order) along the Hexi Corridor over northwestern China. Throughout this dust campaign, the hourly averaged (± standard deviation) aerosol scattering coefficients (σ_{sp}, 550 nm) of the particulates with aerodynamic diameters less than 2.5 μm ($PM_{2.5}$) at these three sites were sequentially 101.5 ± 36.8, 182.2 ± 433.1 and 54.0 ± 32.0 Mm^{-1}. Correspondingly, the absorption coefficients (σ_{ap}, 637 nm) were 9.7 ± 6.1, 6.0 ± 4.6 and 2.3 ± 0.9 Mm^{-1}; single scattering albedos (ω, 637 nm) were 0.902 ± 0.025, 0.931 ± 0.037 and 0.949 ± 0.020; and scattering Ångström exponents ($Å_{sp}$, 450–700 nm) of $PM_{2.5}$ were 1.28 ± 0.27, 0.77 ± 0.51 and 0.52 ± 0.31. During a severe dust storm in Zhangye (i.e., from 23 to 25 April), the highest values of $\sigma_{sp}^{2.5}$ (~5074 Mm^{-1}), backscattering coefficient ($\sigma_{bsp}^{2.5}$, ~522 Mm^{-1}) and ω (~0.993), the lowest values of backscattering fraction ($b_{2.5}$, ~0.101) and $Å_{sp}^{2.5}$ (~–0.046) at 450–700 nm, with peak values of aerosol number size distribution (appearing at the particle diameters range of 1–3 μm) exhibit that the atmosphere aerosols were dominated by coarse mode dust aerosols. It is hypothesized that the relative higher values of MSE during floating dust episodes in Wuwei and Zhangye are attributed to the anthropogenic soil dust produced by agricultural cultivations.

1 Introduction

The role of mineral dust aerosols (MDs) in the climate system has received considerable attention over recent years (Arimoto et al., 2006; Ramanathan et al., 2001). MDs has a profound impact on the radiative balance of the Earth by scattering and absorbing solar radiation (Huang et al., 2010, 2014; Wang et al., 2010; Li et al., 2016); it can also act as cloud condensation nuclei (CCN) to alter the precipitation rate and hydrological cycle of the Earth (Rosenfeld et al., 2001). East Asia includes the Taklimakan, Tengger, Badain Jaran and Gobi Deserts and is thus considered to be one of the major source regions of natural dust in the world, as it produces large amounts of natural mineral dust (Zhang et al., 1997; Wang et al., 2008; Che et al., 2011, 2013; Ge et al., 2014; Xin, 2005, 2010, 2015). The long-range transport of MDs from dust source regions have a significant influence on aerosol radiative forcing and environment changing (Chen et al., 2013; Ge et al., 2011; Liu et al., 2015; Huang et al., 2008). In order to fully account the climate effects of MDs over eastern Asian regions, several international intensive field campaigns were conducted to measure their optical, physical, and chemical properties in recent decades, such as the Asian Aerosol Characterization Experiment (ACE-Asia) (Arimoto et al., 2006), the NASA Global Tropospheric Experiment Transport and Chemical Evolution over the Pacific (TRACE-P) (Jacob et al., 2003), the Atmospheric Brown Clouds-East Asia Regional Experiment (EAREX) (Nakajima et al., 2003), and the 2008 China-U.S. joint dust field experiment (Ge et al., 2010; Li et al., 2010; Wang et al., 2010). For instance, Ge et al. (2010) illustrated the mean single scattering albedo (SSA) measured at Zhangye increases with wavelength from

0.76 ± 0.02 at 415 nm to 0.86 ± 0.01 at 870 nm. Seasonal variations of the scattering coefficients and the absorption coefficients were also collected at Dunhuang and Zhangye of Gansu Province as well as Yulin of Shanxi Province (Li et al., 2010; Xu et al., 2004; Yan et al., 2007). However, the systematic review of the optical and microphysical properties of MDs in eastern Asia is still a challenge due to limited observations, especially for fine mode mineral dust near the dust source areas in northwestern China.

Recently, the potential impacts of anthropogenic soil dust have also received an increasing amount of attention (Prospero et al., 2002; Huang et al., 2015a; Tegen and Fung, 1995; Tegen et al., 2002; Shi et al., 2015; Pu et al., 2015; Wang et al., 2015a). Anthropogenic mineral dust can also influence air quality and human health through the processes of their emission, transport, removal, and deposition (Aleksandropoulou et al., 2011; Chen et al., 2013; Huang et al., 2014, 2015a, 2015b; Kim et al., 2009; Li et al., 2009; Mahowald and Luo, 2003; Zhang et al., 2005, 2015). Ginoux et al. (2010) estimated that anthropogenic dust accounts for 25% of all dust aerosols using observational data from satellite products combined with a land-use fraction dataset. Nie et al. (2014) found observational evidence on new particle formation and growth in heavy dust plumes mixed with anthropogenic pollution via dust-induced heterogeneous photochemical processes. Because anthropogenic dust emissions from disturbed soils are not well constrained, we define anthropogenic dust as mineral dust from areas that have been disrupted by human activities, such as deforestation, overgrazing, and agricultural and industrial activities (Aleksandropoulou et al., 2011; Tao et al., 2014,

2015, 2017; Tegen and Fung, 1995; Tegen et al., 2002, 2004; Thompson et al., 1988); anthropogenic dust is thus different from natural mineral dust, which originates from desert regions (Che et al., 2011, 2013; Goudie and Middleton, 2001; Li et al., 2012; Park and Park, 2014; Pu et al., 2015; Wang et al., 2008, 2010). This assumption is consistent with the results of a recent study by Huang et al. (2015a), who found that anthropogenic dust comprises 91.8% of regional emissions in eastern China and 76.1% of regional emissions in India.

Understanding the natural dust mixed with the anthropogenic aerosols in the troposphere has a critical impact on our ability to get insight into atmospheric compositions and predict global climate change (Nie et al., 2014; Ramanathan et al., 2007; Spracklen and Rap, 2013; Wang et al., 2015b). Although several attempts have been conducted to investigate the significance of the effects of dust on global climate, meteorology, atmospheric dynamics, ecosystems and human health (Rosenfeld et al., 2011; Qian et al., 2004), only limited field campaigns have focused on the properties of the anthropogenic dust aerosols near dust source regions. In this study, we not only focus on the surface measurements of the optical and microphysical properties of anthropogenic dust, but also used statistical analysis to identify the possible signatures of natural dust storms transported from dust source regions over northwestern China.

2 Methodology

2.1 Sites Description

The Hexi Corridor is a ~1000km northwest-southeast-oriented chain of oases in

northwestern China (mainly in the Gansu Province), surrounded by the Qilian Mountains (elevation: ~4000 m), the Beishan Mountains (elevation: ~2500 m), Heli Mountains (elevation: ~2000 m) and the Wushao Mountains (elevation: ~3000 m). The Hexi Corridor is considered to be a heavily polluted area because of the combination of local topography and the human activities occurring over northwestern China (Li et al., 2010; Wang et al., 2010; Bi et al., 2017). The dust field campaign was carried out along the Hexi Corridor from 3 April to 16 May 2014. A ground-based mobile facility of the Semi-Arid Climate and Environment Observatory of Lanzhou University (SACOL) was used in three sites, which was Wuwei (37.72°N, 102.89°E; 1691 m a.s.l.; 3–7 April), Zhangye (39.04°N, 100.12°E; 1578 m a.s.l.; 9–28 April), and Dunhuang (39.96°N, 94.33°E; 1367 m a.s.l.; 3–16 May). The locations of these sites are shown in Figure 1a. As presented in the bottom panels of Figure 1, the Huangyang Farmland in Wuwei (HFW in figures and tables, similarly hereinafter) is located only ~17 km west of the Tengger Desert and ~20 km away from the Qilian Mountains; therefore, anthropogenic air pollutants originating from Wuwei City can directly influence the sampling site because of the prevailing wind direction along the local topography. The Linze farmland in Zhangye (LFZ) is located in northwestern Zhangye City (~30 km), to the southwest of Linze County (~12 km), encompassed by the Qilian Mountains and the Badain Jaran Desert. As shown in Figure 2a and 2b, the site in Wuwei and Zhangye are mainly agricultural fields with similar land surface type, with corn and cotton being the major crops. In general, agricultural and preparation activities were done in April, such as disking, tillage and seeding operations; thus, the local tropospheric aerosols in

Wuwei and Zhangye were dominated by anthropogenic soil dust due to agricultural cultivation activities. However, the sampling site in Dunhuang is located in Gobi Desert (GDD), ~35 km distant from the eastern edge of Kumtag Desert and in the upwind direction of Dunhuang City; there was not any significant anthropogenic pollution source around the mobile facility during the sampling period, and the primary components in Dunhuang were dominated by natural mineral dust (Figure 2c).

2.2 Instrumentation

During the 2014 dust field campaign, ambient temperature (*T*), relative humidity (RH), pressure (*P*), wind direction (WD), and wind speed (WS) were automatically measured with a weather transmitter (model WXT 520, Vaisala Inc., Helsinki, Finland) at 1 min intervals. The aerosol optical and microphysical properties measured at these three sites consist of absorption coefficients (σ_{ap}), total scattering coefficients (σ_{sp}) and backscattering coefficients (σ_{bsp}), mass concentrations, and aerosol number size distribution. The wind direction datasets are associated with the aerosol absorption and scattering coefficients and can be used to determine the origins of natural and anthropogenic dust. Figure 3a shows the ground-based mobile laboratory of SACOL deployed in Dunhuang. The instruments were conducted in the container, where temperature was maintained at 20°C. To minimize local contaminations, a metal sampling stack (10 cm in diameter) was installed at the top of the ground-based mobile laboratory (~6.5 m above the ground level). The airflow was split into several flows and supplied to different instruments, and the particle size cut measurements were

obtained using 1 μm and 2.5 μm impactors, which are shown in Figure 3b. All of the collectors were operated at 50 °C to dry the aerosols (i.e., to a RH of less than 40%). For proper operation under the flow conditions in the present experiments, the internal plumbing of the commercial unit has to be modified once a week. Details of the most relevant instrument's accuracy for aerosol and dust measurements are given in Table 1. Finally, all datasets measured were adjusted to standard temperature and pressure conditions (STP; T=273.15 K, P=101.325 kPa), in which 5 min and hourly averaged data were used.

The mass concentration with the particle diameter (D_p) less than 2.5 μm ($PM_{2.5}$) was measured continuously using an ambient particulate monitor (model RP1400a, R&P Corp., Albany, NY, USA) with a flow rate of 16.7 L min^{-1}, which is based on the principle of tapered element oscillating microbalance (TEOM) (Patashnick and Rupprecht, 1991). We checked the main and auxiliary flow rates of TEOM monitor at least once a week, and the Teflon coated glass fiber filters must be exchanged before the filter loading percentage reaches 60% to ensure the validity of the data generated by the TEOM.

Two integrating nephelometers (model 3563, TSI Inc., Shoreview, MN, USA) with 1 μm and 2.5 μm impactors were also employed to measure the total scattering and backscattering coefficients of aerosol particles at three wavelengths of 450, 550, and 700 nm; the detection limits are 0.44 Mm^{-1}, 0.17 Mm^{-1}, and 0.26 Mm^{-1} (1 Mm^{-1} = 10^{-6} m^{-1}), respectively. The nephelometer has a signal-to-noise ratio (S: N) of 2:1 (Anderson et al., 1996; Shi et al., 2013). The two nephelometers were checked with internally

filtered particle free air once a day and standard CO_2 every two days. CO_2 calibrations were performed before experiment or when CO_2 check error was greater than 5% (Anderson et al., 1996; Anderson and Ogren, 1998). Multiple calibrations following the manufacture's protocol were performed, and the instrument noise was periodically measured throughout this dust field campaign using an inline HEPA (High Efficiency Particulate Air) filter. The datasets collected by nephelometers were corrected for angular nonidealities, which will cause particle scattering in the near forward direction to be underestimated. For reducing and quantifying the uncertainties in aerosol optical properties measured by the nephelometers, the data reduction and uncertainty analysis for the scattering datasets due to nonideal detection are processed following Anderson and Ogren (1998). Combining these errors could yielded a total uncertainty of $\pm$ 8% for a scattering coefficient of 30 Mm^{-1}.

A multi-angle absorption photometer (MAAP, model 5012, Thermo Scientific, Waltham, MA, USA) was used to determine the aerosol absorption coefficients of $PM_{2.5}$ at 637 nm (Müller et al., 2011) with a temporal resolution of 1 min. The detailed description of the MAAP could be found in the literatures (Petzold et al. 2002; Petzold and Schönlinner 2004).

The particle size distribution ranging from 0.5 to 20 μm (52 channels) was measured using an aerodynamical particle sizer (APS) spectrometer (model 3321, TSI Inc., Shoreview, MN, USA), assuming that all aerosols are homogeneous and spherical particles, despite the fact that the observed coarse mode dust particles exhibit non-spherical geometries (Mishchenko et al., 1995). Because of the high aerosol

concentrations (i.e., exceeds 1000 cm^{-3}) when the extreme dust storm outbreak, two diluters (model 3302A, TSI Inc., Shoreview, MN USA) with dilution ratio of 20:1 and 100:1 were used on the top of the APS, and the data has taken account of the dilution ratios and particle loss due to the dilutor.

Although the single particle soot photometer (SP2, DMT Inc., Boulder, CO, USA) was also used to measure the mass concentration and size distribution of black carbon (BC) in Zhangye from 9 to 28 April 2014 during this dust field campaign, the datasets measured by SP2 are used to analyze the mixing status of BC with the other aerosols during this dust field campaign in another manuscript (In preparation). A comparison of the BC mass concentration between SP2 and MAAP instruments is given in Figure S1 in the Supplement. The result indicates that the tendency of BC mass concentrations is much similar, but the values measured by MAAP was relatively larger than that measured by SP2. We note the relative large bias between MAAP and SP2 instruments may result from the size distribution of BC measured by using different sampler inlet impactors of 2.5 μm and 1 μm.

2.3 Data analysis methods

The mass absorption coefficient (MAC) is a key parameter that can be used to attribute the light absorption of aerosols to BC and to understand its effects on climate. Some studies have attempted to perform this attribution based on the assumption of the wavelength dependence of absorption (e.g. Favez et al., 2009; Yang et al., 2009). These values are calculated by assuming that the imaginary part of the complex refractive

index of BC is independent of the wavelength (λ) and that the absorption cross-section of BC varies as λ^{-1} (Bond and Bergstrom, 2006). A narrow range of BC for MAC (6.4–6.6 $m^2\ g^{-1}$) was found to provide a good fit to urban particles collected by previous studies (Arnott et al., 2003; Bond and Bergstrom, 2006; Schwarz et al., 2008), and a value of 6.6 $m^2\ g^{-1}$ is currently used in the MAAP. To calculate the aerosol absorption coefficient at 637 nm, the following equation is used:

$$\sigma_{ap} = \mathrm{MAC} \times m_{BC} \quad (1)$$

where m_{BC} is the equivalent mass concentration of BC reported by the MAAP.

The backscattering fraction (b) is defined as the ratio of aerosol scattering in the backward hemisphere to the total scattering ($b = \sigma_{bsp}/\sigma_{sp}$), and related to particle size distribution. The wavelength-dependent variation of σ_{sp} is characterized by the scattering Ångström exponent (SAE, $Å_{sp}$), which is defined as:

$$Å_{sp}(\lambda_1/\lambda_2) = -\frac{\ln\left(\sigma_{sp,\lambda_1}/\sigma_{sp,\lambda_2}\right)}{\ln\left(\lambda_1/\lambda_2\right)} \quad (2)$$

where σ_{sp,λ_1} and σ_{sp,λ_2} are the aerosol scattering coefficients at wavelengths λ_1 and λ_2, respectively. In this paper, we calculated $Å_{sp}$ from 450 to 700 nm (i.e., using the scattering coefficients measured by nephelometer at 450 and 700 nm).

The aerosol SSA is a key parameter that can be used to investigate the optical and microphysical properties of atmospheric aerosols (Haywood and Shine, 1995), which is defined as the ratio of the scattering coefficient to the total extinction coefficient (i.e., the sum of the scattering and absorption coefficients). To calculate the SSA at 637 nm, we first interpolate the σ_{sp} values to 637 nm using the Ångström law:

$$\sigma_{sp,\,637} = \sigma_{sp,\,550} \times \left(\frac{637}{550}\right)^{-Å_{550\text{-}700}} \quad (3)$$

The SSA (ω) at 637 nm was then calculated using Eq. (4):

$$\omega_{637} = \frac{\sigma_{sp,\,637}}{\sigma_{ap,\,637} + \sigma_{sp,\,637}} \quad (4)$$

Mass scattering efficiency (MSE) is calculated as the slope of the reduced major axis (RMA) linear regression of $\sigma_{sp}^{2.5}$ and $PM_{2.5}$:

$$MSE = \frac{\sigma_{sp}^{2.5}}{PM_{2.5}} \quad (5)$$

where $\sigma_{sp}^{2.5}$ is the aerosol scattering coefficient at 550 nm and $PM_{2.5}$ is the mass concentration measured by TEOM.

In order to estimate the uncertainties of optical properties on our dust aerosol measurements during this dust field campaign, we performed a closure study to compare the $\sigma_{sp}^{2.5}$ measured by nephelometer associated with that calculated based on the particle number size distribution measurements using a modified Mie model. Computer programs based on the Mie theory (Mie, 1908) to calculate scattering of particles are freely available (e.g., BHCOAT, Bohren and Huffman, 1983), and we used an implementation of these algorithms in MATLAB (Mathworks, MA, USA) functions (Mätzler, 2002). Mie scattering calculations of a single spherical particle require the aerosol number size distribution, the aerosol complex refractive index ($m = n+ki$) and the size parameter ($x = \pi D_p/\lambda$) as key input parameters. The scattering coefficients are calculated from the integration of the scattering efficiency (Q_{sp}) over the whole number size distribution:

$$\sigma_{sp}(x,m) = \int_{D_p} Q_{sp}(x,m) \cdot \frac{\pi D_p^{\,2}}{4} \cdot N(\log D_p) \cdot d\log D_p \quad (6)$$

where D_p is the particle diameter, and $N(\log D_p)$ represents number-size distribution

measured by the APS. In this study, the real part of the refractive index (n) was assumed to be 1.53, which was widely used for mineral dust in literatures (Müller et al., 2009; McConnell et al., 2010); the imaginary part of the refractive index (k) was determined using Mie calculations.

3 Results

3.1 Temporal Variability

Floating dust is generally defined as a weather phenomenon in which fine mode dust particles suspended in the lower troposphere under calm or low-wind condition, with horizontal visibility less than 10 km; while dust storm is that large quantities of dust particles lofted by strong winds, and horizontal visibility reduced to below 1 km. (Wang et al., 2005; Wang et al., 2008). During this dust field campaign, three floating dust episodes (which are shown as dotted boxes in Figure 4) occurred on 3–7 April in Wuwei and on 9–12 and 25–28 April in Zhangye. We also observed the optical and microphysical properties of natural mineral dust during a heavy dust storm (shown as a solid box in Figure 4) from 23 to 25 April in Zhangye. Moreover, we identified five clear-sky days in Zhangye (16, 18, 19, 20 and 22 April) and three clear-sky days in Dunhuang (11, 14 and 15 May) as background weather conditions based on the manual weather recording and the abovementioned measurements. According to the land surface types shown in Figure 2, one of the major novelties of this study is to investigate the characteristics of anthropogenic and natural dust during floating dust and dust storms episodes, respectively. Figure 4 illustrates the temporal variations of hourly

averaged σ_{sp}, σ_{bsp}, σ_{ap}, b, ω, as well as $Å_{sp}$, MSE, and aerosol size distribution in Wuwei, Zhangye, and Dunhuang in chronological order from 3 April to 16 May 2014. Note that the time periods denoted in Figure 4 contain some gaps due to the transportation of ground-based mobile facility or instrument problems. The statistical analyses of the optical parameters are also summarized in Table 2. Hereinafter, these results are given as the mean ± the standard deviation of the hourly averaged datasets. Unless otherwise noted, all aerosol scattering measurements discussed here are for the wavelength of 550 nm.

Aerosol optical and microphysical properties are entirely different in these three sites. One of the most significant features in Figure 4a is that the variation of $\sigma_{sp}^{2.5}$ is highly consistent with that of $\sigma_{sp}^{1.0}$ during the whole period of field campaign; the backscatter coefficients shows the same trends with the total scattering coefficients but in a relatively small magnitude. The values of $\sigma_{sp}^{2.5}$ and $\sigma_{sp}^{1.0}$ are very close in Wuwei and Zhangye; however, the large differences observed in Dunhuang. It indicates that fine mode particles dominate the scattering coefficient in farmland regions, whereas coarse mode particles play a more important role in the desert regions. Except for the values obtained during a heavy dust storm, the hourly mean $\sigma_{sp}^{2.5}$ are 101 ± 37 Mm^{-1} and 84 ± 58 Mm^{-1} at two anthropogenically influenced sites in Wuwei and Zhangye, respectively; the corresponding $\sigma_{bsp}^{2.5}$ are 12.2 ± 4.4 Mm^{-1} and 9.5 ± 5.9 Mm^{-1}. By contrast, the much lower $\sigma_{sp}^{2.5}$ (54.0 ± 32.0 Mm^{-1}) and $\sigma_{bsp}^{2.5}$ (6.5 ± 3.7 Mm^{-1}) are measured in Dunhuang. Values for $b_{2.5}$ are 0.121 ± 0.005, 0.115 ± 0.007 and 0.122 ± 0.005 in Wuwei, Zhangye, and Dunhuang, respectively, which are consistent

with the result in Backgarden (0.124 ± 0.015; Garland et al., 2008), a rural site near the megacity Guangzhou in southeastern China, but higher than those observed in Shouxian in eastern China (0.101 ± 0.017; Fan et al., 2010).

Meanwhile, the large standard deviations of $\sigma_{ap}^{2.5}$ are found in Wuwei and Zhangye, which are possibly attribute to frequent floating dust events and local anthropogenic emissions (Wang et al., 2008, 2015a). The lowest value of $\sigma_{ap}^{2.5}$ during the field campaign (2.3 ± 0.9 Mm^{-1}) are obtained in Dunhuang, which can be compared with the relative higher σ_{ap} values of 9.7 ± 6.0 Mm^{-1} and 5.5 ± 3.8 Mm^{-1} in Wuwei and Zhangye, respectively. This observation reveals that natural mineral dust is still a weaker absorber than anthropogenic soil dust that has been mixed with air pollutants. Compared with Figure 4b, Figure 4d indicates that the majority of ω_{637} values are much higher in Dunhuang than that in the other two sites, where these values range from ~0.874 to 0.986, with overall mean value of 0.949 ± 0.020. Similar results were also found in other field campaigns in Zhangye (ω_{550} of 0.95 ± 0.02; Li et al., 2010) and Yulin (ω_{530} of 0.95 ± 0.05; Xu et al., 2004). By contrast, only 0.7 % and 21.9 % of the values reach up to 0.95 in Wuwei and Zhangye (except for the dust storm period, as shown in Figure 7), and their average values are much lower (0.902 ± 0.025 and 0.925 ± 0.034, respectively) and also exhibit larger variation. This phenomenon most likely indicates that natural dust aerosols dominated in Dunhuang absorb less than other atmospheric aerosols. The overall average MSE values in Wuwei, Zhangye and Dunhuang are 2.79 ± 0.57 m^2 g^{-1}, 2.21 ± 0.64 m^2 g^{-1} and 1.55 ± 0.59 m^2 g^{-1}, with maximum values of 4.37 m^2 g^{-1}, 4.49 m^2 g^{-1}, and 3.57 m^2 g^{-1}, respectively. The higher

MSE values in Wuwei and Zhangye reflect the fact that anthropogenic dust, which is influenced by local soil dust during floating dust episodes, scatters more solar radiation than natural dust (Figure 4f).

Aerosol size distribution (hereinafter defined as $dN/d\log D_p$) in the range of 0.5–5 μm is also presented in Figure 4g, which indicates that fine mode particles (typically $D_p < \sim 1$ μm) are dominant in Wuwei and Zhangye. The number concentration of coarse mode particles (typically $D_p > \sim 1$ μm) is higher than that of fine mode particles in Dunhuang (calculated from the integral of the size distribution curve), this region yields hourly averaged number concentration of 7.2 cm^{-3} and 9.0 cm^{-3} for fine mode and coarse mode particles, respectively, with the average percentage of coarse mode particles relative to total atmospheric particles of ~55%, which is higher than the relative percentages observed in Wuwei (~16 %) and Zhangye (~33 %).

On 23–25 April 2014, a severe dust storm occurred in Zhangye, along with a strong northerly wind. The hourly averaged $\sigma_{sp}^{2.5}$ value increased remarkably from ~186 to 5074 Mm^{-1}, which is 10 times higher than that measured in non-dust plume periods in Zhangye (~509 Mm^{-1}); while the maximum value of $\sigma_{ap}^{2.5}$ is ~37.6 Mm^{-1} during this dust storm, which is slightly higher than that measured during non-dust plume periods (~36.0 Mm^{-1}). Figures 4d and 4e delineate that the peaks of ω_{637} (> 0.99) associated with the negative values of $Å_{sp}$ (< 0) are close to those observed in another field campaign over northwestern China (Li et al., 2010), which is possibly related to the reduce of anthropogenic emissions and the prevalence of coarse mode particles (Cermak et al., 2010). Figure 4g demonstrates that the values of aerosol number size

distribution peaked at 1–3 μm. Simultaneously, the number concentration of coarse mode particles generally exceed 300 cm^{-3} and even approach 1200 cm^{-3}, which reveals that pure coarse mode particles from desert regions are dominant during the dust storm. These results are consistent with those of a previous study, in which the aerosol diameter of PM_{10} was determined to be larger during dust plume periods than it was during non-dust plume periods (Wang et al., 2010).

3.2 Diurnal Variations

Here, we also present the diurnal cycles of $\sigma_{sp}^{2.5}$, $\sigma_{sp}^{1.0}$, $\sigma_{ap}^{2.5}$ and ω_{637}, as well as those of $Å_{sp}$ and MSE values in Wuwei (red lines), Zhangye (black lines), and Dunhuang (blue lines) throughout the experiment (Figure 5). As shown in Figure 5a and 5b, the values of $\sigma_{sp}^{2.5}$, $\sigma_{sp}^{1.0}$ and $\sigma_{ap}^{2.5}$ present prominent bimodal distributions in Wuwei and Zhangye, which are consistent with the variations in ω_{637} (Figure 5c). The maximal $\sigma_{ap}^{2.5}$ value (~16.8 Mm^{-1}) appeared at 08:00 LST (local standard time) in Wuwei, with two secondary peak values occurring at 21:00 (~20.2 Mm^{-1}) and 22:00 LST (~18.7 Mm^{-1}). Similarly, two comparable peaks of $\sigma_{ap}^{2.5}$ appeared at 08:00 (~12.2 Mm^{-1}) and 20:30 (~9.7 Mm^{-1}) LST in Zhangye. It is indicate that not only anthropogenic mineral dust but also local air pollutants (e.g., BC and OC) were found in Wuwei and Zhangye; these pollutants likely originated from agricultural activities, biomass burning, and the burning of fossil fuels (e.g., domestic coal combustion, diesel emissions from vehicles). The pronounced diurnal variations in these sites may also associated with the local meteorological elements (Arya, 1999). Compared with the lower ω_{637} values that

occurred at ~19:30–20:30 (~0.880) and ~07:30 LST (~0.864) in Wuwei and Zhangye, respectively, the higher ω_{637} with only slight variations in Dunhuang indicates that natural dust aerosols are dominant near the dust source areas (Figure 5e). Additionally, there are large diurnal variations of $Å_{sp}^{2.5}$ and $Å_{sp}^{1.0}$ in Wuwei, ranging from ~1.0–1.7 and ~1.8–2.3, respectively; these lowest values observed in Dunhuang could partly support the conclusion that its atmospheric aerosols are dominated by pure coarse mode particles (Figure 5c–5d). Large diurnal variations in MSE are also found at all three sites; MSE values is the lowest in Dunhuang because of the amounts of pure coarse mode particles near the source areas (Figure 5f).

As is shown in Figure 6a, the accumulated fine mode particles increased in Wuwei, yielding a maximum number distribution concentration of more than 100 cm^{-3} due to the frequent outbreaks of floating dust episodes that occurred on 3–7 April 2014. The similar pattern of fine mode particles is found in Zhangye, but with a slightly lower number distribution of fine mode particles (Figure 6b). We suggest that the fine mode particles represent the dominant contributions in Wuwei and Zhangye, which is due to the formation of local anthropogenic soil dust by agricultural cultivations.

Figure 7 shows the histograms of the single scattering albedo values in these three sites. During the floating dust period in Wuwei, the majority of the ω_{637} values of fine mode particles that originated from anthropogenic soil dust range from ~0.900–0.925; approximately 10–20 % of those values range from ~0.875–0.900 and ~0.925–0.950. The overall range of ω_{637} values observed in Zhangye is similar to that observed in Wuwei. The ω_{637} values that range from ~0.900–0.925 are 30 % higher than those in

Zhangye. This result is consistent with that of Li et al. (2010), who noted that the SSA of a dust storm was approximately 0.98 for coarse mode particles, while lower SSA values (i.e., ranging from 0.89 to 0.91) were closely related to local air pollution. Thus, we infer that the atmospheric aerosols in Wuwei and Zhangye not only include anthropogenic soil dust that is smaller than 1 μm but also have undergone mixing with air pollutants during their transportation from urban and industrial regions. However, the ω_{637} values in Dunhuang range from ~0.925–0.975, with the majority of these values falling between ~0.950–0.975 because of the high percentage of coarse mode particles. These results are consistent with that of a previous study, which indicated that the surface measurement of SSA for coarse mode particles from Saharan desert regions at 550 nm yielded a value of 0.97 $\pm$ 0.02 (Cattrall et al., 2003).

3.3 Local Emission Sources Attribution

Additionally, the wind roses described in Figure 8 can be used to provide further insights into the correlation between the meteorology and local emission sources. The wind direction accompanying $\sigma_{sp}^{2.5}$ and $\sigma_{ap}^{2.5}$ most likely represents the emissions from both local sources and regional transport from remote regions. The dominant wind directions in these three sites are generally more abundant to the west. Figure 8a indicate that the higher values of $\sigma_{sp}^{2.5}$ (> 160 Mm^{-1}) are found along with the south wind, which implies that dust particles are primarily generated from nearby farmlands; the majority of $\sigma_{ap}^{2.5}$ values are dominated by the southeast wind because of the emissions of anthropogenic pollutants from the Huangyang Town. The fact that the

highest values of $\sigma_{sp}^{2.5}$ (> 140 Mm^{-1}) and $\sigma_{ap}^{2.5}$ (> 12 Mm^{-1}) are associated with the west wind in Zhangye most likely indicates that anthropogenic soil dust mixed with local air pollutants from their upwelling residences (Figure 8c and 8d). However, both $\sigma_{sp}^{2.5}$ and $\sigma_{ap}^{2.5}$ are probably influenced by coarse mode mineral dust origin from desert areas due to the prevalent northwest wind in Dunhuang (Figure 8e and 8f).

MSE is a key parameter that can be used to estimate the radiative forcing effects due to atmospheric particles on global climate. Therefore, several studies have been performed to determine the optical properties of aerosols using MSE values (Laing et al., 2016). For instance, Hand and Malm (2007) noted that the MSE is mainly dependent on particle composition (e.g., the particle refractive index and aerosol size distribution). As shown in Figure 9a, coarse mode particles have significantly higher ω_{637} (> 0.93) and lower MSE (1 < MSE < 2) values because of the presence of natural mineral dust under background weather condition in Dunhuang. However, there appears to be no clear difference between the ω_{637} and MSE values due to floating dust periods in Wuwei and Zhangye. The presence of lower MSE in Wuwei and higher values in Zhangye, suggests that fine mode particles can not only be attributed to floating dust periods (due to local soil dust) but also include BC, OC and other air pollutants that originated from the burning of biomass and fossil fuels. For instance, the large variations in ω_{637} and MSE observed in Wuwei and Zhangye are consistent with values that were previously measured during dust storms or biomass burning events (Li et al., 2010; Laing et al., 2016). Another notable feature is the remarkable discrepancy between the optical properties of aerosols for a given type of aerosol with diameters of

less than 1 μm and 2.5 μm. Although the values of $\sigma_{sp}^{1.0}$ measured during this dust field campaign are only slightly lower than those of $\sigma_{sp}^{2.5}$ (as is indicated in Figures 9b and 9c), the $Å_{sp}^{1.0}$ values range from ~1.4–2.3 (mean: 2.1) for fine mode particles because of floating dust episodes in Wuwei, compared to the values of $Å_{sp}^{2.5}$ range from ~0.5–1.7 (mean: 1.3) observed during the same period in Wuwei. Similar results are also found at the other two sites in Zhangye and Dunhuang.

3.4 Case study

Aerosol optical depth (AOD) is a major optical parameter for aerosol particles and a key factor affecting global climate (Holben et al., 1991, 2001, 2006; Srivastava and Bhardwaj, 2014). Dubovik et al. (2002) demonstrated that non-spherical mineral dust can be retrieved using the assumption of spherical aerosols for high aerosol loading (AOD >0.5, Å <0.7) in desert regions due to dust events. Figure 10 illustrates the spatial distribution of deep blue AOD at 550 nm in East Asia retrieved using Terra-MODIS during a heavy dust storm over northern China on 24 April 2014. During this dust storm, the spatial distribution of high aerosol loadings with AOD values of >1.6 over northwest China was observed; in this distribution, the transport of natural mineral dust from the Taklimakan Desert to the downwelling regions over China can be clearly seen. The most prominent feature in Figure 11 is that $\sigma_{sp}^{2.5}$ reaches its peak value of ~5074 Mm^{-1} and that a strong relationship (R^2 = 0.9093) existed between $\sigma_{sp}^{2.5}$ and $\sigma_{ap}^{2.5}$ during the dust storm. However, the values of $\sigma_{ap}^{2.5}$ observed during the dust storm are consistent with those measured during floating dust episodes in Wuwei and Zhangye.

Therefore, we note that large differences in $\sigma_{sp}^{2.5}$ between natural mineral dust and anthropogenic soil dust because of the presence of fine mode particles during floating dust episodes and coarse mode particles during dust storms. We also observed the lowest values of $\sigma_{ap}^{2.5}$ and $\sigma_{sp}^{2.5}$ (which range from ~1.2–7.9 Mm^{-1} and ~16–224 Mm^{-1}, respectively) in Dunhuang, which indicates that natural mineral dust represents the dominant particles under the background condition.

Figure 12 shows the average aerosol number size distribution observed under different weather conditions during this field campaign. These data clearly show that the dominant particles during the dust storm in Zhangye are coarse mode particles ranging in size from 1 μm to 5 μm, which peaked at 1.60 μm with a maximum $dN/d\log D_p$ value of ~590 cm^{-3}. Compared with dust storms, the $dN/d\log D_p$ reaches a peak with values of ~336 cm^{-3} and ~332 cm^{-3} at 0.67 μm during typical floating dust episodes on 4–7 in Wuwei and 9–12 April in Zhangye, respectively. This observation indicates that fine mode anthropogenic soil dust mixed with local air pollutants was dominant during these two floating dust episodes. However, another floating dust episode that occurred in Zhangye reveals a bimodal variation, which peaked at 0.67 μm and 1.49 μm. It also should be noted that the lowest value of $dN/d\log D_p$ for fine mode particles was observed in Dunhuang under the background weather condition. These results are very close to those of previous studies that stated that atmospheric particles were dominated by both anthropogenic soil dust and air pollutants during floating dust episodes; however, the amount of coarse mode particles increased sharply during natural dust storms that originated from dust source regions (Wang et al., 2010;

Li et al., 2010).

The gravimetric density of fine mode particles is reported to range from 1.00–2.00 g cm^{-3}, with an average value of 1.5 g cm^{-3} (Sloane et al., 1991; Seinfeld and Pandis, 1998). In this study, the gravimetric density of fine mode mineral dust particles was estimated by using the integrated volume concentrations measured by APS and the mass concentration of $PM_{2.5}$ measured by TEOM. As shown in Figure S2 and Table 3, we found that the gravimetric density of dust particles is in the range of 1.04 to 1.64 g cm^{-3}, and there is no evidence of significant differences of the dust gravimetric density during floating dust and dust storm episodes. Then, the volume-weighted mean diameters (VMD) under the diameter of 2.5 μm and 1.0 μm are also calculated by using the integrated number size distribution of APS data (DeCarlo et al., 2005). We found that the $VMD_{2.5}$ and $\text{Å}_{sp}^{2.5}$ are correlated well during the whole dust field campaign (Figure S3 in Supplement). However, there is no significant linear correlation between $VMD_{1.0}$ and $\text{Å}_{sp}^{1.0}$. The highly possible explanation is that the $VMD_{1.0}$ is calculated based on the aerosol size diameter ranging from ~0.5 to 1 μm measured by APS, while the variation of $\text{Å}_{sp}^{1.0}$ is affected by the aerosol diameter under 1 μm.

Finally, we use the Mie theory and the aerosol number size distribution to estimate the scattering coefficient compared with that derived by the nephelometer. As shown in Figure 13, the Mie-calculated scattering coefficient ($\sigma_{sp,\,Mie}$) and the measured scattering coefficient ($\sigma_{sp,\,neph}^{2.5}$) of 550 nm are highly correlated. For instance, the imaginary part of the refractive index (0.001) for natural dust during dust storm in Zhangye and the background weather condition in Dunhuang are similar to the result

of SAMUM-1 in Saharan (Müller et al., 2009). However, the higher value of imaginary part (~0.01–0.08) during floating dust reflects inherently more anthropogenic dust particles, which can absorb more solar radiation than that during dust storm. Based on the Mie calculation in this study, the $PM_{2.5}$ scattering fraction, which defined as the contribution of the light scattering of $PM_{2.5}$ to the total scattering (the calculated scattering coefficient in the size range of 0.5–20 μm), is ~36.4 % during dust storm, while is in the range of ~37.9–85.1 % during floating dust episode. Detailed information of Mie-calculated and measured scattering coefficient is summarized in Table 3. Comparisons between $\sigma_{sp,\,Mie}$ and $\sigma_{sp,\,neph}$ were carried out taking into account the uncertainties of the measurements and the calculations. The $\sigma^{2.5}_{sp,\,Mie}$ is ~6.6% higher than $\sigma^{2.5}_{sp,\,neph}$ during dust storm, while ~16.5% lower than that during floating dust from 9 to 12 April. Generally, most of the $\sigma^{2.5}_{sp,\,Mie}$ agree well with $\sigma^{2.5}_{sp,\,neph}$, which can reflect a good quality of the datasets of $\sigma^{2.5}_{sp}$ during this dust field campaign.

4 Conclusions

This study is novel in that we not only captured natural mineral dust near the desert regions but also characterized the properties of anthropogenic soil dust produced by agricultural cultivations, especially during floating dust episodes. The most prominent conclusion is that there are significant differences in the optical and microphysical properties of aerosols between anthropogenic soil dust and natural mineral dust under different atmospheric conditions (e.g., dust storm, floating dust episodes and background conditions). During the floating dust period in Wuwei (i.e., 3–7 April), the

average values of $\sigma_{sp}^{2.5}$, $\sigma_{bsp}^{2.5}$, $\sigma_{ap}^{2.5}$, ω_{637}, $Å_{sp}^{2.5}$ and MSE are 102 ± 37 Mm^{-1}, 12.2 ± 4.4 Mm^{-1}, 9.7 ± 6.1 Mm^{-1}, 0.902 ± 0.025, 1.28 ± 0.27 and 2.79 ± 0.57 $m^2 g^{-1}$, respectively; during two floating dust periods in Zhangye (i.e., 9–12 and 25–28 April), the corresponding values are 115 ± 36 Mm^{-1}, 12.1 ± 4.2 Mm^{-1}, 6.4 ± 4.0 Mm^{-1}, 0.935 ± 0.030, 0.73 ± 0.59 and 2.24 ± 0.57 $m^2 g^{-1}$, respectively; whereas these values are sequentially 1088 ± 991 Mm^{-1}, 114.6 ± 101.6 Mm^{-1}, 10.6 ± 7.6 Mm^{-1}, 0.989 ± 0.004, –0.014 ± 0.018 and 1.73 ± 0.20 $m^2 g^{-1}$ during dust storms in Zhangye (i.e., 23–25 April). The number size distribution ($dN/d\log D_p$) of coarse mode particles with diameters of 1–3 μm can reach a peak of ~590 cm^{-3}, which reveals that pure coarse mode particles from desert regions were dominant during dust storms in Zhangye. However, the overall variations of ω_{637}, which ranges from ~0.82–0.95 and ~0.83–0.98 during floating dust episodes in Wuwei and Zhangye, respectively, indicate that atmospheric aerosols not only include anthropogenic soil dust that is smaller than 1 μm but has also undergone mixing with air pollutants because of their transportation from urban and industrial regions. We note that the values of $\sigma_{sp}^{1.0}$ (74 ± 27 Mm^{-1}) are only slightly lower than those of $\sigma_{sp}^{2.5}$ (101 ± 37 Mm^{-1}) that are observed in Wuwei.

We used a modified Mie theory and the aerosol number size distribution measured by APS to estimate the scattering coefficients. The imaginary parts of the refractive indexes for natural dust during dust storm in Zhangye and the background weather condition in Dunhuang are 0.001, while the higher value of imaginary part (0.01–0.08) during floating dust reflects inherently more anthropogenic dust particles, which reflects that these atmospheric aerosols during this dust field campaign not only were

dominated by anthropogenic soil dust produced by agricultural cultivations in Wuwei and Zhangye, but also underwent natural mineral dust originated from the dust source regions over northwestern China.

5 Data availability

All data sets and codes used to produce this study can be obtained by contacting Xin Wang (wxin@lzu.edu.cn). The MODIS data used in this study are available at Aerosol Product, https://modis.gsfc.nasa.gov/data/dataprod/mod04.php.

Competing interests. The authors declare that they have no conflict of interest.

Acknowledgements. This research was supported by the Foundation for Innovative Research Groups of the National Science Foundation of China (41521004), the National Science Foundation of China under Grant (41775144 and 41522505). The MODIS data were obtained from the NASA Earth Observing System Data and Information System.

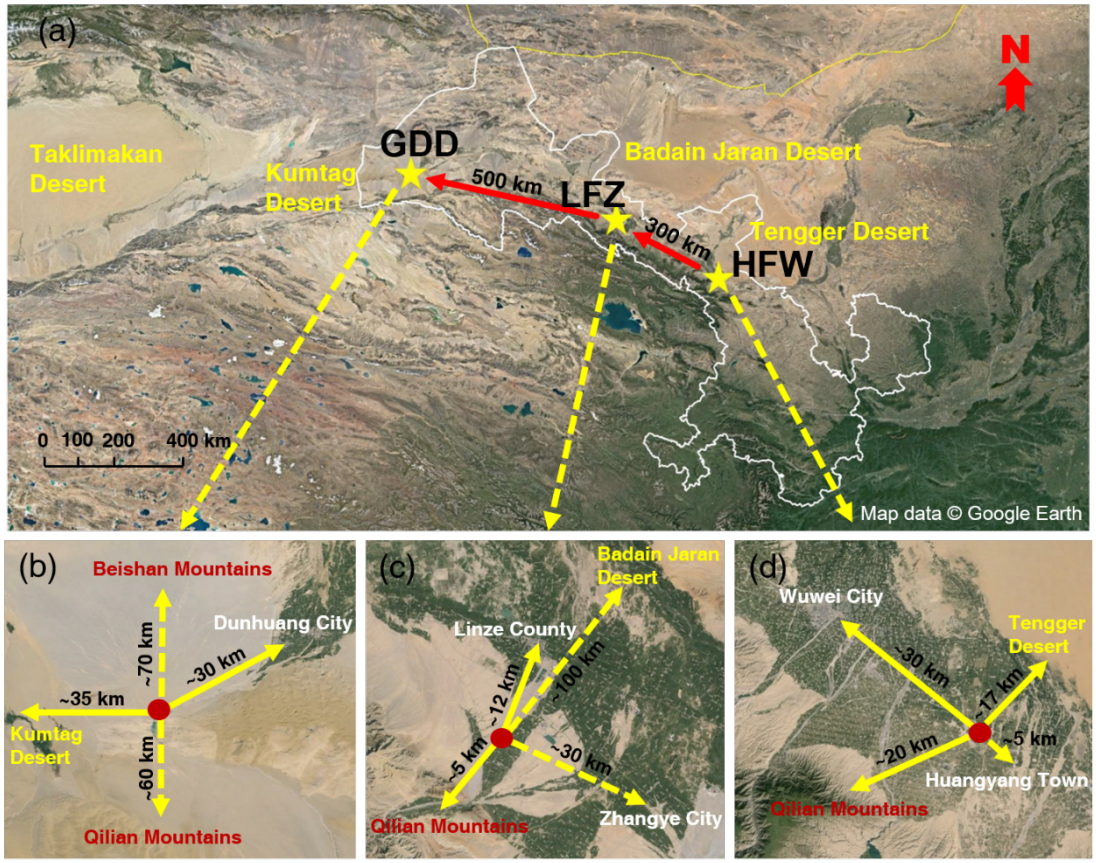

Figure 1. (a) The sampling locations of ground-based mobile laboratory and their surrounding areas near dust source regions during the 2014 dust field campaigns at **(b)** Gobi Desert in Dunhuang (GDD, 39.96°N, 94.33°E; 1367 m a.s.l.), **(c)** Linze Farmland in Zhangye (LFZ, 39.04°N, 100.12°E; 1578 m a.s.l.) and **(d)** Huangyang Farmland in Wuwei (HFW, 37.72°N, 102.89°E; 1691 m a.s.l.).

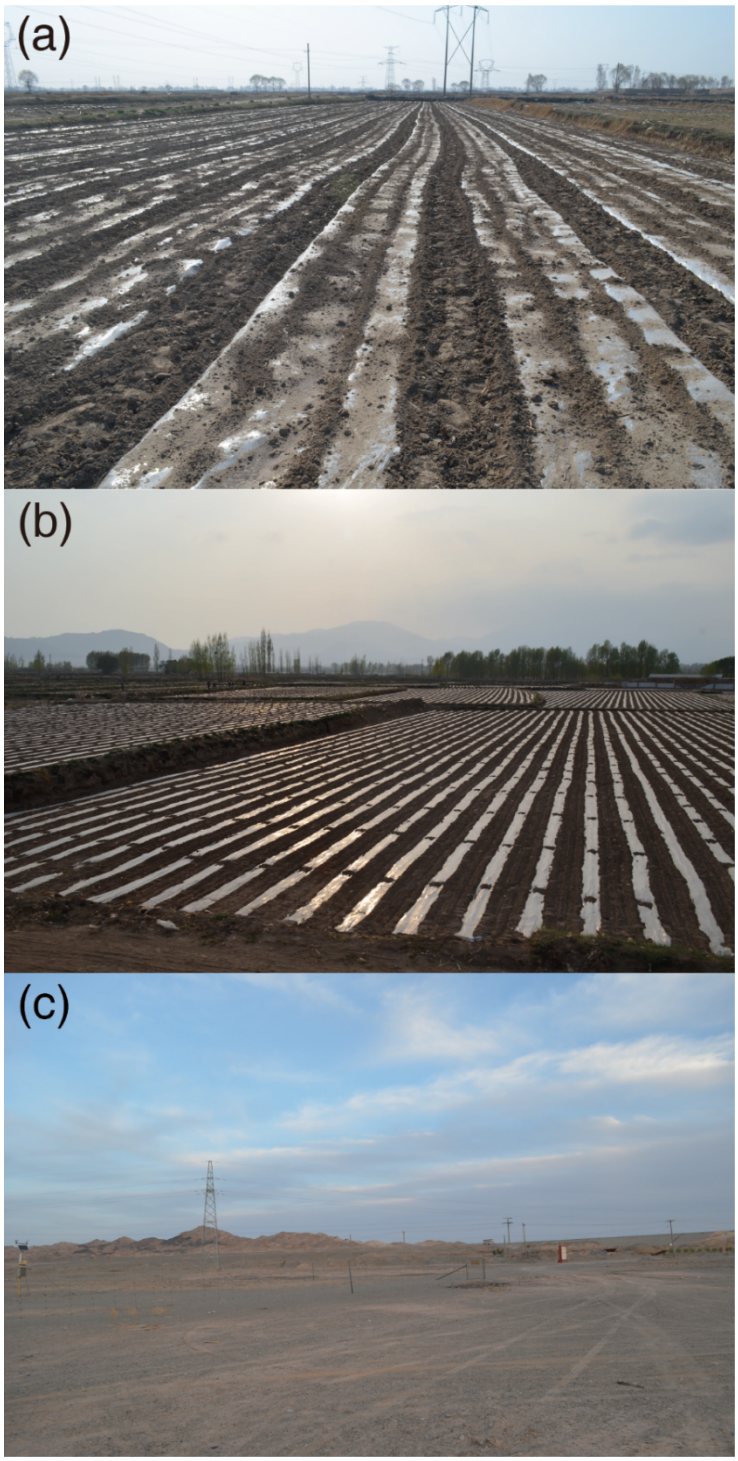

Figure 2. Same as **Figure 1** but for land surface conditions at **(a)** Huangyang Farmland in Wuwei (HFW), **(b)** Linze Farmland in Zhangye (LFZ), and **(c)** Gobi Desert in Dunhuang (GDD).

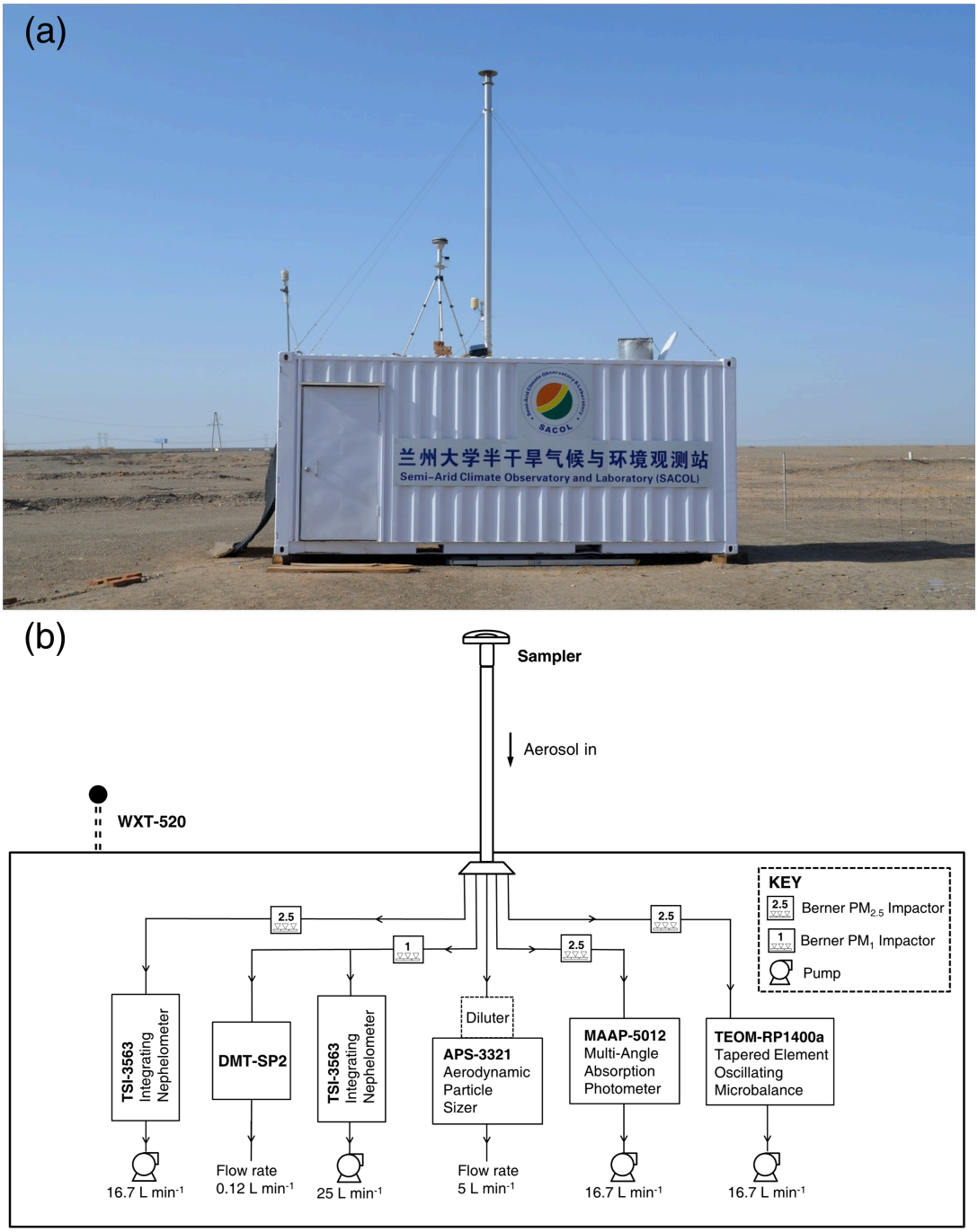

Figure 3. (a) The ground-based mobile laboratory in Dunhuang and **(b)** the schematic diagram of the ensemble instrumentation system.

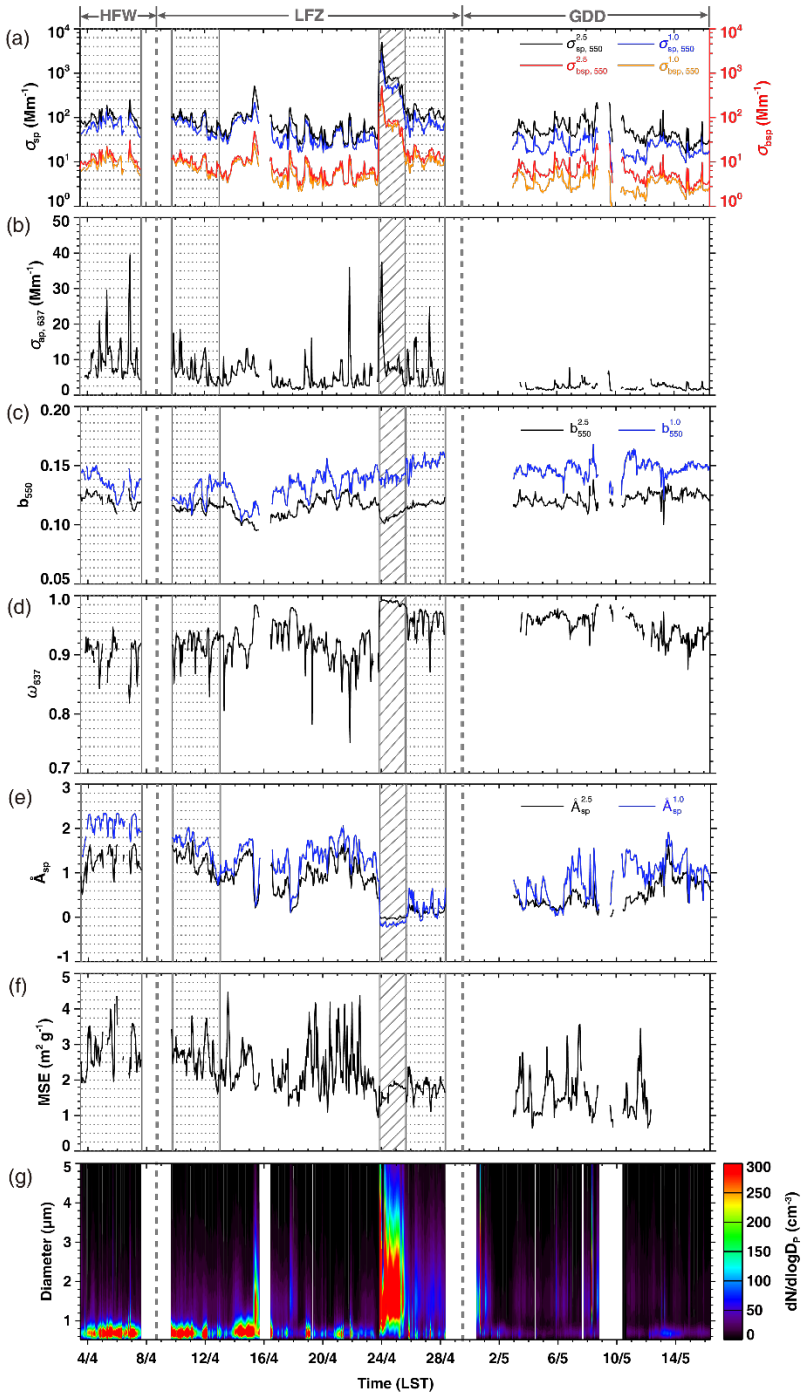

Figure 4. Temporal variations of hourly averaged **(a)** aerosol scattering coefficient at 550 nm and absorption coefficient at 637nm, **(b)** the backscattering fractions at 550 nm **(c)** single scattering albedo at 637 nm, **(d)** scattering Ångström exponent (calculated from 450 nm to 700 nm), **(e)** mass scattering efficiency (MSE) of $PM_{2.5}$ at 550 nm, and **(f)** aerosol size distribution ($dN/d\log D_p$, 0.5 $\mu m < D_p < 5$ μm) during the entire period from 3 April to 16 May 2014. The shaded box represents a strong dust storm that occurred in Zhangye, and the dotted boxes represent three floating dust episodes that occurred in Wuwei and Zhangye.

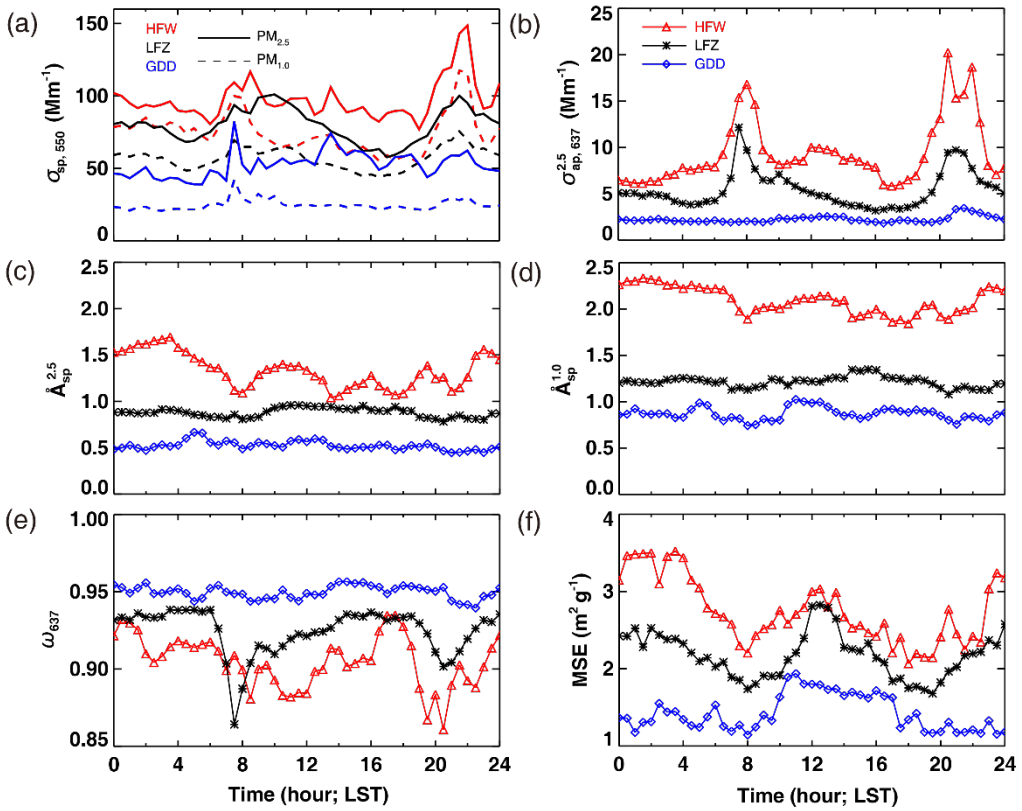

Figure 5. Diurnal variations in **(a)** aerosol scattering coefficient at 550 nm, where solid lines represent the variations of $PM_{2.5}$ and dotted lines represent the variations of $PM_{1.0}$; **(b)** the aerosol absorption coefficient at 637 nm and the scattering Ångström exponent for **(c)** $PM_{2.5}$ and **(d)** $PM_{1.0}$ (both calculated from 450 to 700 nm); **(e)** single scattering albedo at 637 nm; and **(f)** mass scattering efficiency (MSE) at 550 nm in Wuwei, Zhangye, and Dunhuang from 3 April to 16 May 2014. Note that data collected during the strong dust storm in Zhangye are excluded.

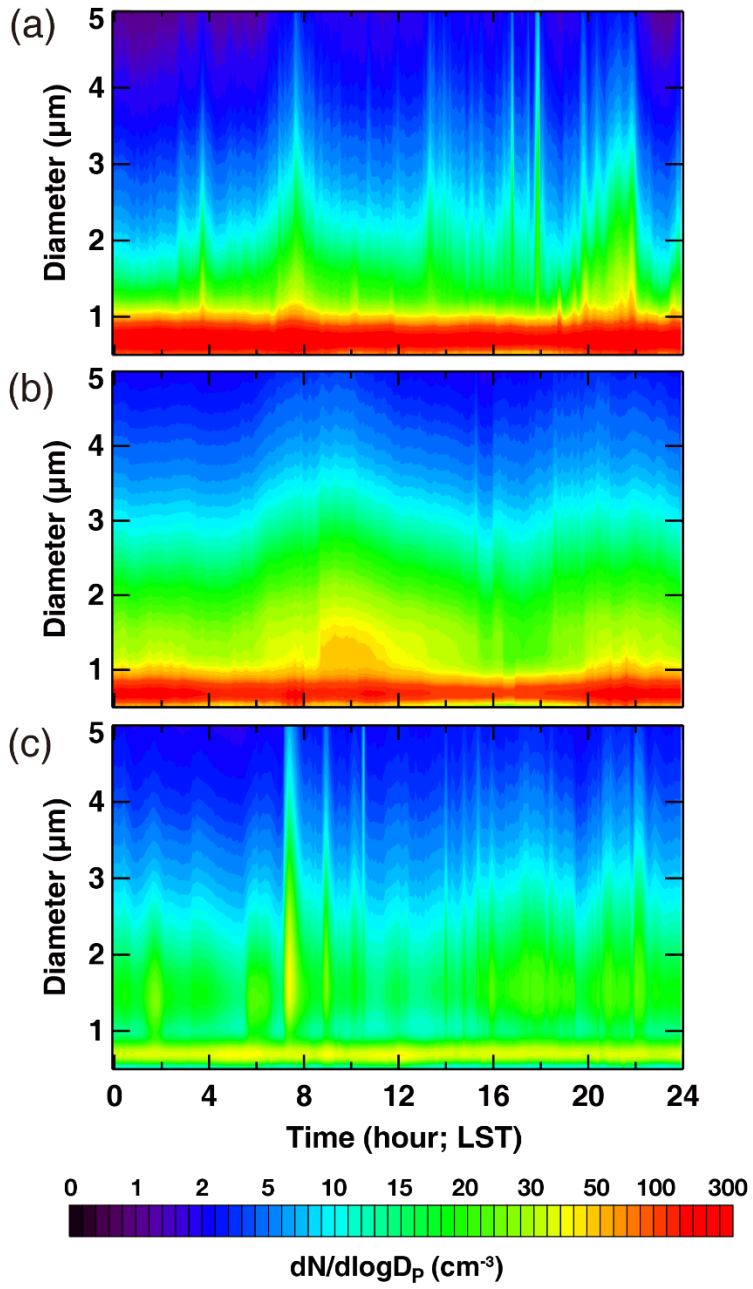

Figure 6. Same as **Figure 5** but for aerosol size distribution (dN/dlogD_p , 0.5 μm < D_p < 5 μm) in **(a)** Wuwei, **(b)** Zhangye, and **(c)** Dunhuang from 3 April to 16 May 2014. Note that data collected during the strong dust storm in Zhangye are excluded.

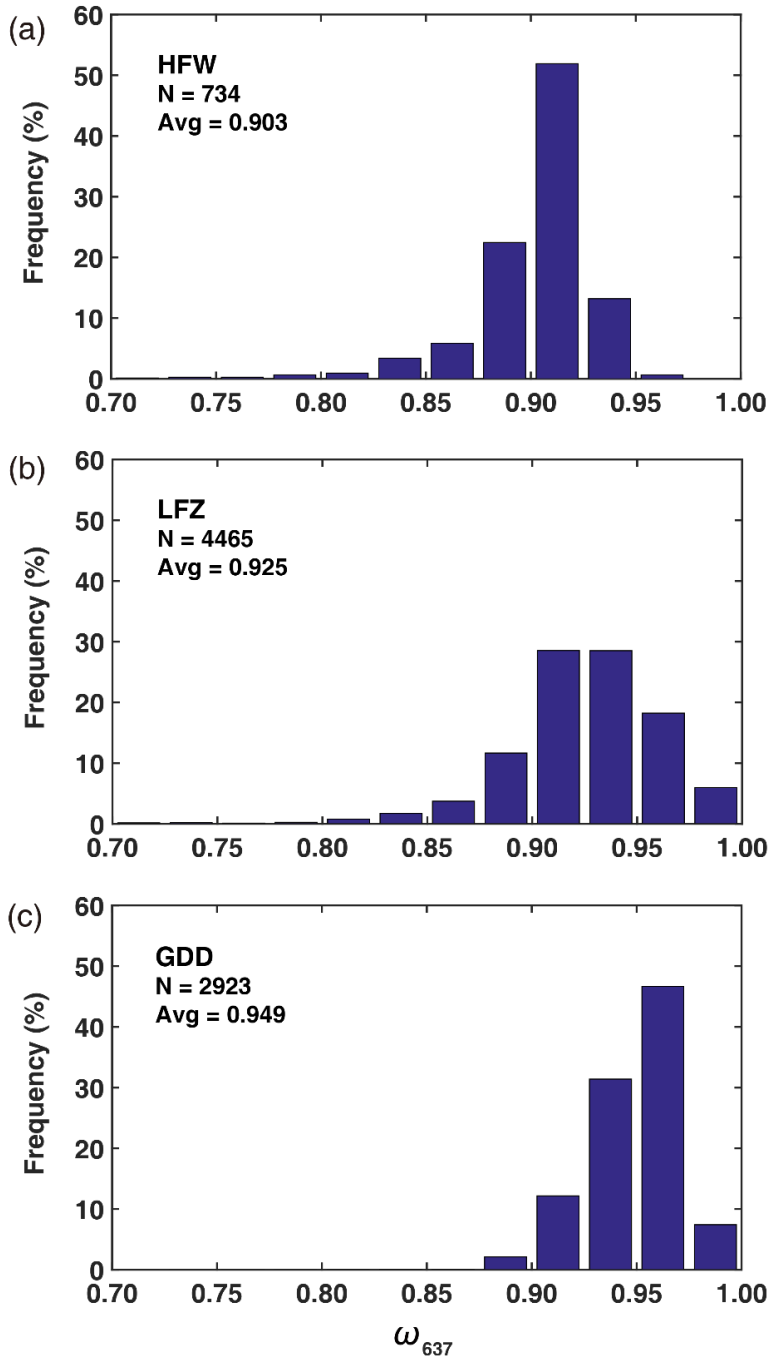

Figure 7. Histograms of 5 min averaged single scattering albedo at 637 nm in **(a)** Wuwei, **(b)** Zhangye, and **(c)** Dunhuang. The numbers of samples and average values are also shown. Note that data collected during the strong dust storm in Zhangye are excluded.

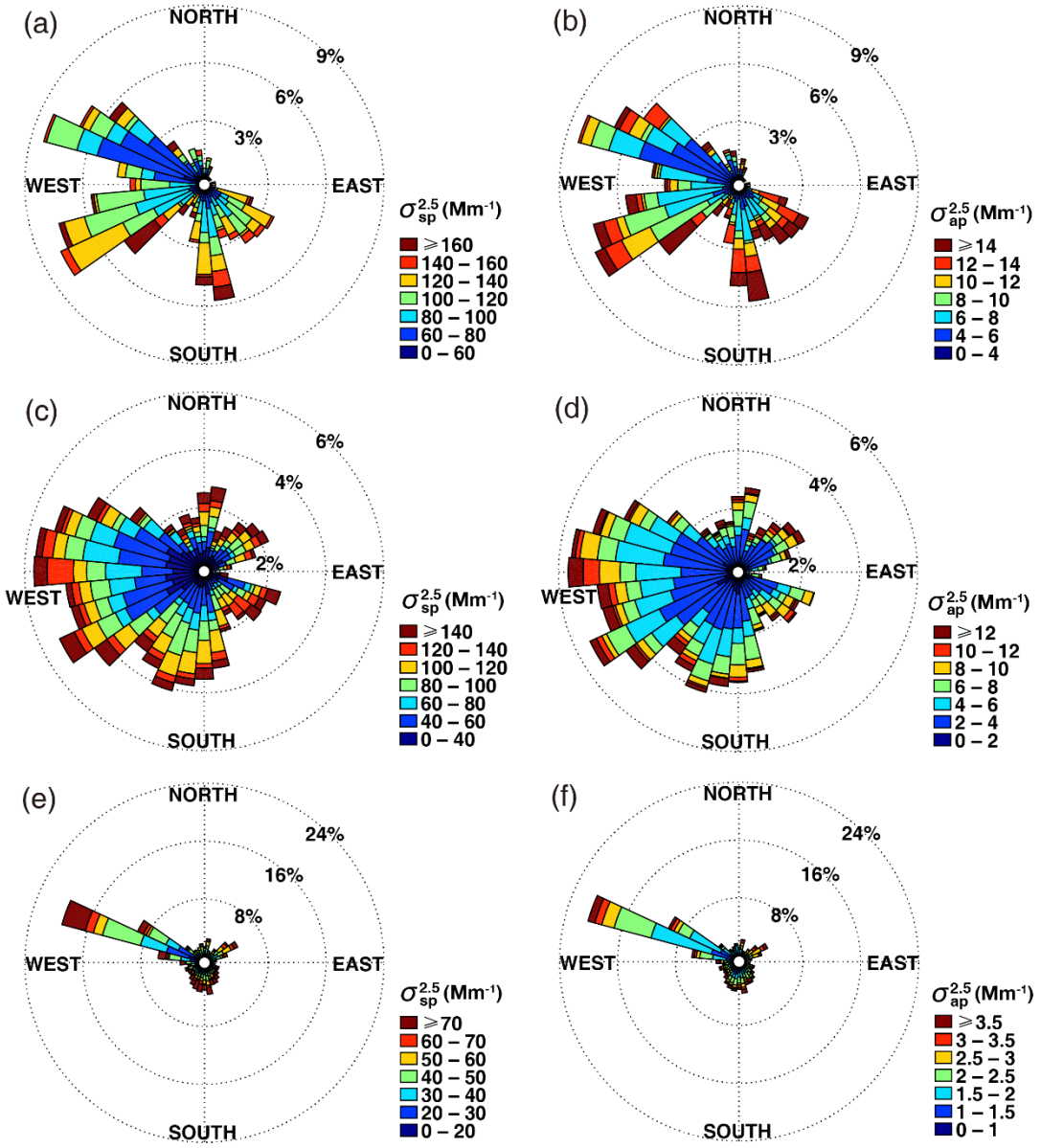

Figure 8. Wind roses for **(a)** aerosol scattering coefficient at 550 nm and **(b)** aerosol absorption coefficient at 637 nm in Wuwei; **(c)** and **(d)** are the same as **(a)** and **(b)** but for Zhangye; and **(e)** and **(f)** are the same as **(a)** and **(b)** but for Dunhuang. Note that data collected during the strong dust storm in Zhangye are excluded.

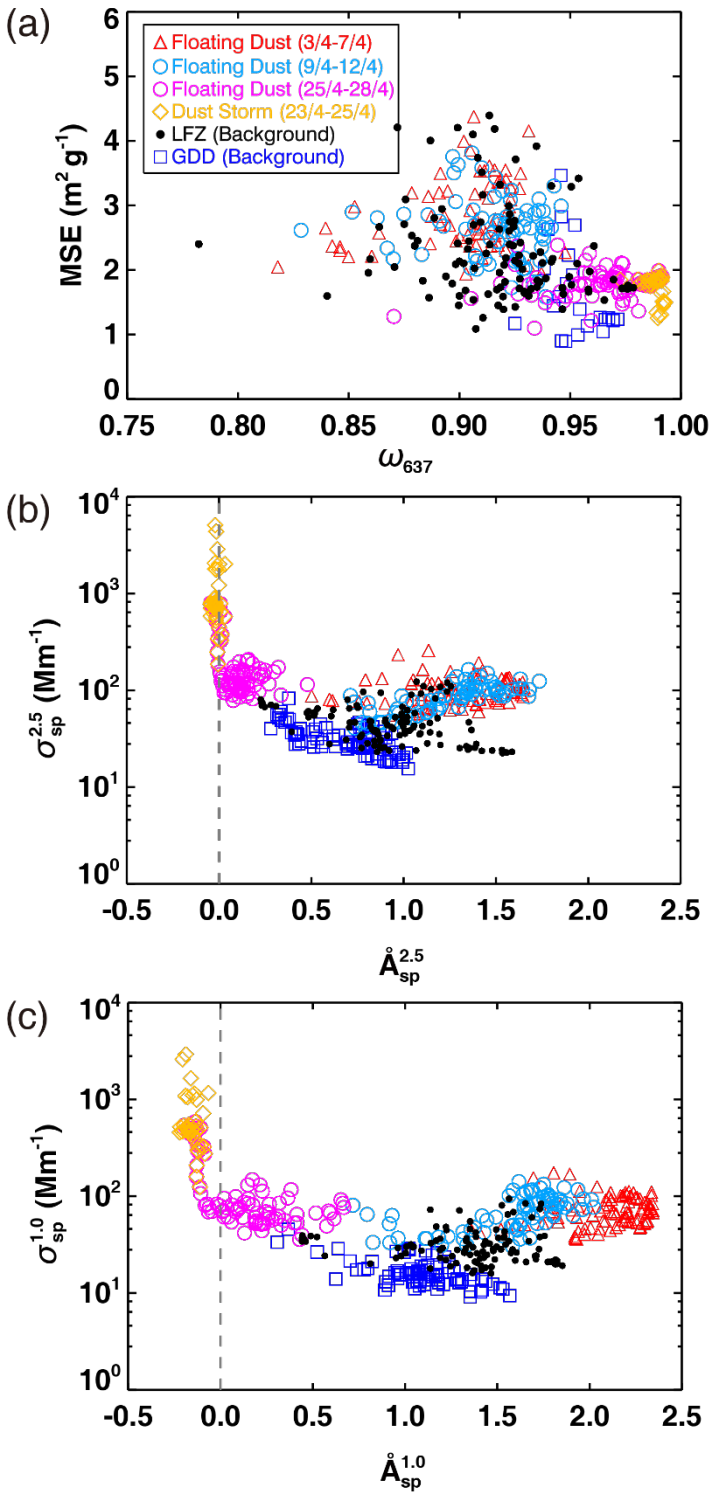

Figure 9. Scatter plots of **(a)** mass scattering efficiency (MSE) versus single scattering albedo (ω) at 637 nm and **(b)** scattering Ångström exponent at 450–700 nm versus aerosol scattering coefficient of $PM_{2.5}$ at 550 nm; **(c)** is the same as **(b)** but for $PM_{1.0}$. The color symbols represent different atmospheric conditions during the dust field campaign.

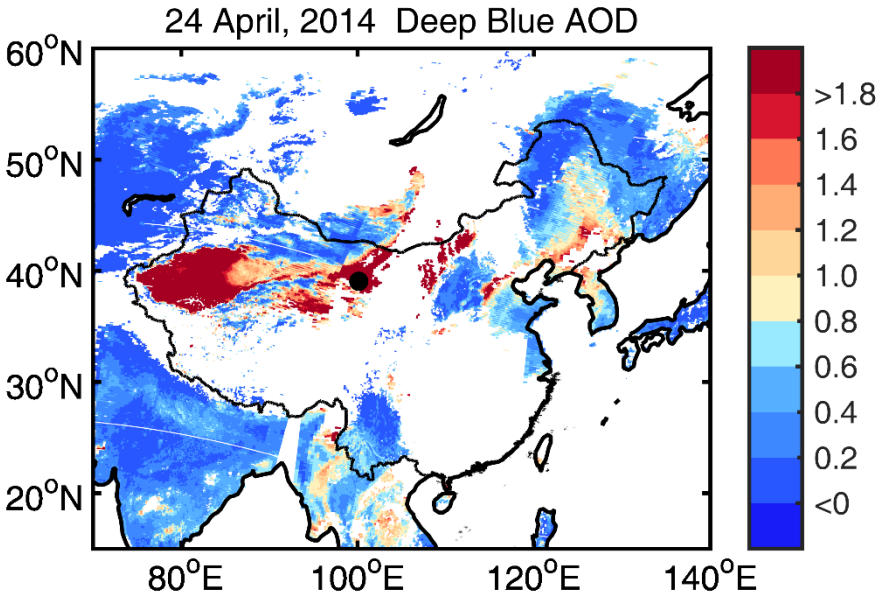

Figure 10. Terra MODIS Deep Blue AOD measured at 550 nm by the NASA Giovanni system during a heavy dust storm on 24 April 2014. The black dot represents the location of the ground-based mobile laboratory at Zhangye.

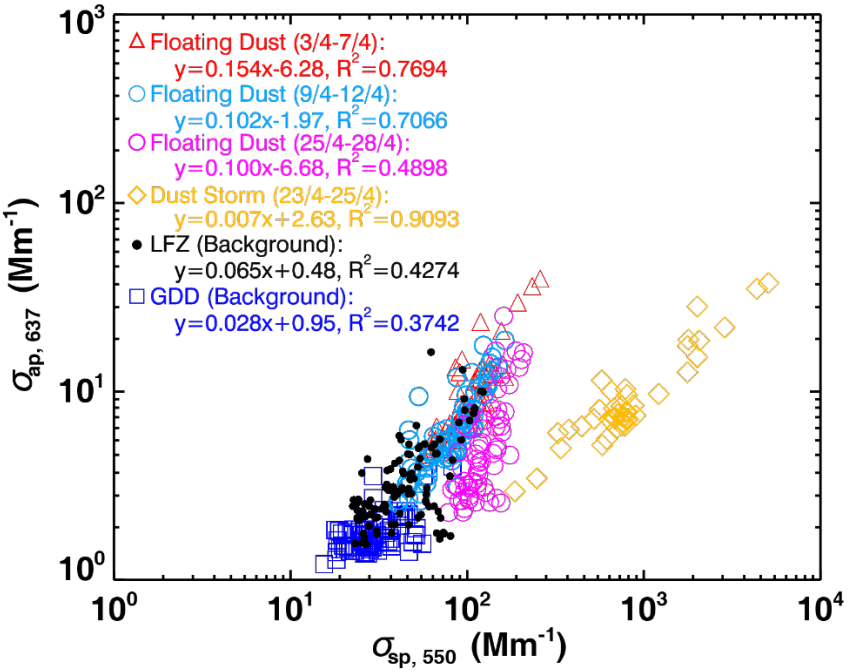

Figure 11. Scatter plot of aerosol absorption coefficients versus scattering coefficients from 3 April to 16 May 2014. The color symbols represent different atmospheric conditions during the dust field campaign.

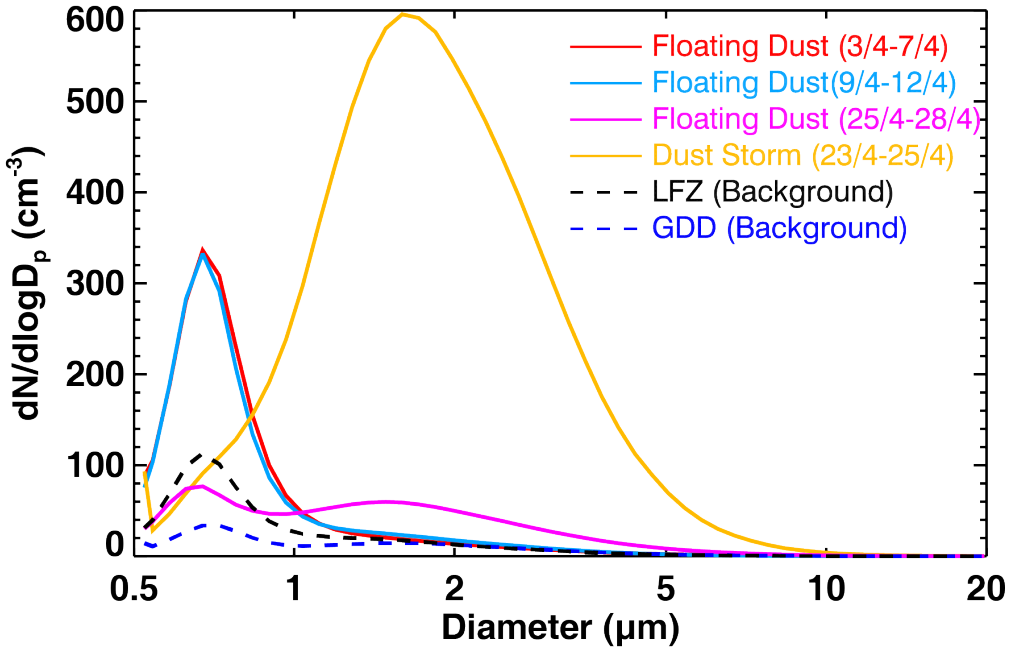

Figure 12. Average aerosol size distribution (dN/dlogD_p, cm^{-3}) based on all run data collected under different weather conditions during the entire campaign.

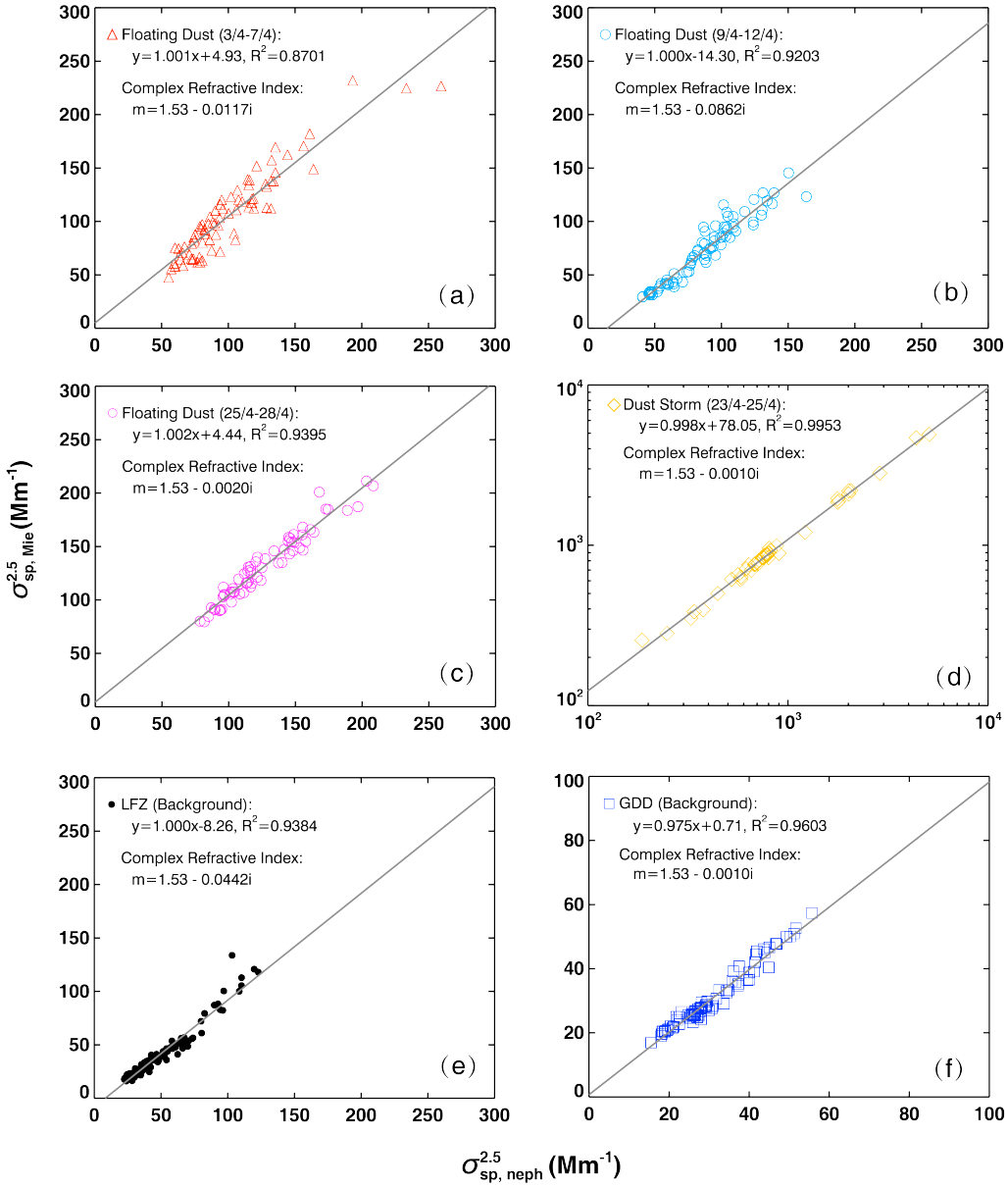

Figure 13. Correlation between $PM_{2.5}$ scattering coefficient calculated from Mie Theory and observed by the nephelometer at 550nm under different atmospheric conditions during the dust field campaign.

Table 1. The main aerosol observations and ground-based instrumentations at three sites.

Observation	Instrumentation	Model & manufacturer	Accuracy
Meteorological elements	Weather transmitter	WXT 520, Vaisala, Helsinki, Finland	T: ± 0.3; RH: 0.1 %; P: 0.1 hPa; WS: 0.1 m s^{-1}; WD: 1°
$PM_{2.5}$ concentration	Ambient particulate monitor	RP1400a, R&P Corp., Albany, NY, USA	0.1 μg m^{-3}
Aerosol total scattering/backscattering coefficient	Integrating nephelometer	TSI 3563, TSI Inc., Shoreview, MN, USA	0.44, 0.17, and 0.26 Mm^{-1} at the wavelengths of 450, 550, and 700 nm, respectively
Aerosol absorption coefficient	Multi-angle absorption photometer	MAAP 5012, Thermo Scientific, Waltham, MA, USA	0.66 Mm^{-1}
Aerosol size distribution	Aerodynamic particle sizer	APS 3321, TSI Inc., Shoreview, MN, USA	0.001 cm^{-3}

Table 2. Statistics of optical properties of aerosols measured at the three sites from 3 April to 16 May 2014 .Results are given as the mean ± the standard deviation, which based on hourly averaged data.

	λ (nm)	HFW	LFZ			GDD
			All	Non-dust	Dust storm	
$\sigma_{sp}^{1.0}$ (Mm^{-1})	450	109.7 ± 39.4	125.0 ± 240.8	70.7 ± 39.2	626.1 ± 520.1	28.8 ± 11.6
	550	74.0 ± 27.2	117.0 ± 254.0	57.2 ± 32.5	668.0 ± 559.2	23.9 ± 11.1
	700	43.5 ± 16.4	104.7 ± 259.1	43.1 ± 26.8	673.0 ± 566.5	20.7 ± 11.4
$\sigma_{sp}^{2.5}$ (Mm^{-1})	450	132.7 ± 47.3	193.1 ± 422.7	98.3 ± 62.0	1068.4 ± 971.8	58.9 ± 31.5
	550	101.5 ± 36.8	182.2 ± 433.1	84.3 ± 58.1	1087.1 ± 990.8	54.0 ± 32.0
	700	75.6 ± 28.4	168.8 ± 430.9	70.5 ± 54.5	1076.8 ± 979.7	49.1 ± 31.7
$\sigma_{bsp}^{1.0}$ (Mm^{-1})	450	12.8 ± 4.7	16.7 ± 34.8	8.5 ± 4.3	92.3 ± 76.5	4.0 ± 1.7
	550	9.9 ± 3.6	15.8 ± 35.3	7.5± 3.9	92.9 ± 77.4	3.5 ± 1.6
	700	7.8 ± 2.7	15.6 ± 36.5	6.9 ± 4.0	95.5 ± 79.6	3.3 ± 1.6
$\sigma_{bsp}^{2.5}$ (Mm^{-1})	450	15.3 ± 5.5	22.0 ± 48.5	10.9 ± 6.6	124.0 ± 110.1	7.6 ± 4.0
	550	12.2 ± 4.4	19.7 ± 44.9	9.5 ± 5.9	114.6 ± 101.6	6.5 ± 3.7
	700	11.2 ± 4.0	19.8 ± 46.7	9.1 ± 6.0	118.8 ± 105.5	6.5 ± 3.8
$\sigma_{ap}^{2.5}$ (Mm^{-1})	637	9.7 ± 6.1	6.0 ± 4.6	5.5 ± 3.8	10.6 ± 7.6	2.3 ± 0.9
ω	637	0.902 ± 0.025	0.931 ± 0.037	0.925 ± 0.034	0.989 ± 0.004	0.949 ± 0.020
$b_{1.0}$	450	0.117 ± 0.009	0.126 ± 0.018	0.123 ± 0.017	0.148 ± 0.004	0.137 ± 0.007
	550	0.135 ± 0.009	0.135 ± 0.013	0.134 ± 0.013	0.140 ± 0.003	0.147 ± 0.007
	700	0.181 ± 0.007	0.161 ± 0.012	0.163 ± 0.011	0.143 ± 0.003	0.159 ± 0.012
$b_{2.5}$	450	0.115 ± 0.007	0.113 ± 0.008	0.113 ± 0.008	0.118 ± 0.003	0.131 ± 0.004
	550	0.121 ±0.005	0.114 ± 0.007	0.115 ± 0.007	0.107 ± 0.003	0.122 ± 0.005
	700	0.150 ± 0.007	0.131 ± 0.012	0.133 ± 0.011	0.113 ± 0.003	0.136 ± 0.010
$Å_{sp}^{1.0}$	450–700	2.09 ± 0.22	1.05 ± 0.66	1.18 ± 0.56	–0.15 ± 0.04	0.87 ± 0.42
$Å_{sp}^{2.5}$	450–700	1.28 ± 0.27	0.77 ± 0.51	0.86 ± 0.47	–0.01 ± 0.02	0.52 ± 0.31

MSE (m^2 g^{-1})	550	2.79 ± 0.57	2.21 ± 0.64	2.26 ± 0.65	1.73 ± 0.20	1.55 ± 0.59

Table 3. Statistical summary of optical and microphysical properties of aerosols in different atmospheric conditions during the dust field campaign.

	Floating Dust (3/4–7/4)	Floating Dust (9/4–12/4)	Floating Dust (25/4–28/4)	Dust Storm (23/4–25/4)	LZF (Background)	GDD (Background)
Dust particle density (g cm^{-3})	1.32 ± 0.28	1.04 ± 0.17	1.24 ± 0.21	1.16 ± 0.51	1.33 ± 0.44	1.64 ± 0.50
Refractive index	1.53–0.0117*i*	1.53–0.0862*i*	1.53–0.0020*i*	1.53–0.0010*i*	1.53–0.0442*i*	1.53–0.0010*i*
$\sigma_{sp,\ neph}^{2.5}$ (Mm^{-1})	102 ± 37	86 ± 29	127 ± 31	1087 ± 991	49 ± 24	31 ± 9
$\sigma_{sp,\ Mie}^{2.5}$ (Mm^{-1})	107 ± 40	72 ± 30	132 ± 32	1163 ± 992	41 ± 25	31 ± 9
$\sigma_{sp,\ Mie}^{20}$ (Mm^{-1})	153 ± 51	102 ± 31	334 ± 75	2983 ± 2712	66 ± 32	71 ± 27
$PM_{2.5}$ scattering fraction (%)	49.3	85.1	37.9	63.6	74.8	43.7

References

Aleksandropoulou, V., Torseth, K., and Lazaridis, M.: Atmospheric Emission Inventory for Natural and Anthropogenic Sources and Spatial Emission Mapping for the Greater Athens Area, Water Air Soil Pollut., 219, 507–526, doi:10.1007/s11270-010-0724-2, 2011.

Anderson, T. L., Covert, D. S., Marshall, S. F., Laucks, M. L., Charlson, R. J.,

Waggoner, A. P., Ogren, J. A., Caldow, R., Holm, R. L., Quant, F. R., Sem, G. J., Wiedensohler, A., Ahlquist, N. A., and Bates, T. S.: Performance characteristics of a high-sensitivity, three-wavelength total scatter-backscatter nephelometer, J. Atmos. Ocean. Tech., 13, 967–986, 1996.

Anderson, T. L. and Ogren, J. A.: Determining aerosol radiative properties using the TSI 3563 Integrating Nephelometer, Aerosol Sci. Tech., 29, 57–69, doi:10.1080/02786829808965551, 1998.

Arimoto, R., Kim, Y. J., Kim, Y. P., Quinn, P. K., Bates, T. S., Anderson, T. L., Gong, S., Uno, I., Chin, M., Huebert, B. J., Clarke, A. D., Shinozuka, Y., Weber, R. J., Anderson, J. R., Guazzotti, S. A., Sullivan, R. C., Sodeman, D. A., Prather, K. A., and Sokolik, I. N.: Characterization of Asian Dust during ACE-Asia, Global Planet. Change, 52, 23–56, doi:10.1016/j.gloplacha.2006.02.013, 2006.

Arnott, W. P., Moosmuller, H., Sheridan, P. J., Ogren, J. A., Raspet, R., Slaton, W. V., Hand, J. L., Kreidenweis, S. M., and Collett, J. L.: Photoacoustic and filter-based ambient aerosol light absorption measurements: Instrument comparisons and the role of relative humidity, J. Geophys. Res-Atmos, 108, 4034, doi:10.1029/2002jd002165, 2003.

Arya, S. P.: Air Pollution Meteorology and Dispersion, 310 pp., Oxford University Press, New York, 1999.

Bi, J., Huang, J., Shi, J., Hu, Z., Zhou, T., Zhang, G., Huang, Z., Wang, X., and Jin, H.: Measurement of scattering and absorption properties of dust aerosol in a Gobi farmland region of northwestern China–a potential anthropogenic influence, Atmos. Chem. Phys., 17, 7775–7792, doi:10.5194/acp-17-7775-2017, 2017.

Bohren, C. F. and Huffman, D. R.: Absorption and Scattering of Light by Small Particles, John Wiley, Hoboken, N. J., 1983.

Bond, T. C. and Bergstrom, R. W.: Light Absorption by Carbonaceous Particles: An Investigative Review, Aerosol Sci. Tech., 40, 27–67, doi:10.1080/02786820500421521, 2006.

Cattrall, C., Carder, K. L., and Gordon, H. R.: Columnar aerosol single-scattering albedo and phase function retrieved from sky radiance over the ocean: measurements of Saharan dust, J. Geophys. Res.-Atmos., 108, 4287, doi:10.1029/2002jd002497, 2003.

Cermak, J., Wild, M., Knutti, R., Mishchenko, M. I., and Heidinger, A. K.: Consistency of global satellite-derived aerosol and cloud data sets with recent brightening observations, Geophys. Res. Lett., 37, 5, doi:10.1029/2010gl044632, 2010.

Che, H. Z., Wang, Y. Q., and Sun, J. Y.: Aerosol optical properties at Mt. Waliguan Observatory, China, Atmos. Environ., 45, 6004–6009, doi:10.1016/j.atmosenv.2011.07.050, 2011.

Che, H. Z., Wang, Y. Q., Sun, J. Y., Zhang, X. C., Zhang, X. Y., and Guo, J. P.: Variation of Aerosol Optical Properties over the Taklimakan Desert in China, Aerosol Air Qual. Res., 13, 777–785, doi:10.4209/aaqr.2012.07.0200, 2013.

Chen, S. Y., Huang, J. P., Zhao, C., Qian, Y., Leung, L. R., and Yang, B.: Modeling the transport and radiative forcing of Taklimakan dust over the Tibetan Plateau: A case study in the summer of 2006, J. Geophys. Res.-Atmos., 118, 797–812,

doi:10.1002/jgrd.50122, 2013.
DeCarlo, P. F., Slowik, J. G., Worsnop, D. R., Davidovits, P., and Jimenez, J. L.: Particle morphology and density characterization by combined mobility and aerodynamic diameter measurements. Part 1: Theory, Aerosol Sci. Tech., 38, 1185–1205, doi:10.1080/02786820590928897, 2005.
Dubovik, O., Holben, B. N., Eck, T. F., Smirnov, A., Kaufman, Y. J., King, M. D., Tanré, D., and Slutsker, I.: Variability of absorption and optical properties of key aerosol types observed in worldwide locations, J. Atmos. Sci., 59, 590–608, 2002.
Fan, X. H., Chen, H. B., Xia, X. G., Li, Z. Q., and Cribb, M.: Aerosol optical properties from the Atmospheric Radiation Measurement Mobile Facility at Shouxian, China, J. Geophys. Res.-Atmos, 115, 13, doi:10.1029/2010jd014650, 2010.
Favez, O., Cachier, H., Sciare, J., Sarda-Esteve, R., and Martinon, L.: Evidence for a significant contribution of wood burning aerosols to PM2.5 during the winter season in Paris, France, Atmos. Environ., 43, 3640–3644, doi:10.1016/j.atmosenv.2009.04.035, 2009.
Garland, R. M., Yang, H., Schmid, O., Rose, D., Nowak, A., Achtert, P., Wiedensohler, A., Takegawa, N., Kita, K., Miyazaki, Y., Kondo, Y., Hu, M., Sha, M., Zeng, L. M., Zhang, Y. H., Andreae, M. O., and Poschl, U.: Aerosol optical properties in a rural environment near the mega-city Guangzhou, China: implications for regional air pollution, radiative forcing and remote sensing, Atmos. Chem. Phys., 8, 5161–5186, doi:10.5194/acp-8-5161-2008, 2008.
Ge, J. M., Huang, J. P., Xu, C. P., Qi, Y. L., and Liu, H. Y.: Characteristics of Taklimakan dust emission and distribution: A satellite and reanalysis field perspective, J. Geophys. Res.-Atmos., 119, 11772–11783, doi:10.1002/2014jd022280, 2014.
Ge, J. M., Su, J., Ackerman, T. P., Fu, Q., Huang, J. P., and Shi, J. S.: Dust aerosol optical properties retrieval and radiative forcing over northwestern China during the 2008 China-U.S. joint field experiment, J. Geophys. Res-atmos, 115, doi:10.1029/2009jd013263, 2010.
Ge, J. M., Su, J., Fu, Q., Ackerman, T. P., and Huang, J. P.: Dust aerosol forward scattering effects on ground-based aerosol optical depth retrievals, J. Quant. Spectrosc. Ra., 112, 310–319, doi:10.1016/j.jqsrt.2010.07.006, 2011.
Ginoux, P., Garbuzov, D., and Hsu, H. C.: Identification of anthropogenic and natural dust sources using Moderate Resolution Imaging Spectroradiometer (MODIS) Deep Blue level 2 data, J. Geophys. Res.-Atmos., 115, D05204, doi:10.1029/2009jd012398, 2010.
Goudie, A. S. and Middleton, N. J.: Saharan dust storms: Nature and consequences, Earth-Sci. Rev., 56, 179–204, doi:10.1016/S0012-8252(01)00067-8, 2001.
Hand, J. L. and Malm, W. C.: Review of aerosol mass scattering efficiencies from ground-based measurements since 1990, J. Geophys. Res.-Atmos., 112, D16203, doi:10.1029/2007jd008484, 2007.
Haywood, J. M., and Shine, K. P.: The Effect of Anthropogenic Sulfate and Soot Aerosol on the Clear-Sky Planetary Radiation Budget, Geophys. Res. Lett., 22, 603–606, doi:10.1029/95gl00075, 1995.

Holben, B. N., Eck, T. F., and Fraser, R. S.: Temporal and Spatial Variability of Aerosol Optical Depth in the Sahel Region in Relation to Vegetation Remote-Sensing, Int. J. Remote Sens., 12, 1147–1163, doi: 10.1080/01431169108929719, 1991.

Holben, B. N., Eck, T., Slutsker, I., Smirnov, A., Sinyuk, A., Schafer, J., Giles, D., and Dubovik, O.: AERONET Version 2.0 quality assurance criteria, in: Remote Sensing of the Atmosphere and Clouds, Proc. of SPIE, Goa, India, 13–17 November, 6408, doi:10.1117/12.706524, 2006.

Holben, B. N., Tanre, D., Smirnov, A., Eck, T. F., Slutsker, I., Abuhassan, N., Newcomb, W. W., Schafer, J. S., Chatenet, B., Lavenu, F., Kaufman, Y. J., Castle, J. V., Setzer, A., Markham, B., Clark, D., Frouin, R., Halthore, R., Karneli, A., O'Neill, N. T., Pietras, C., Pinker, R. T., Voss, K., and Zibordi, G.: An emerging ground-based aerosol climatology: Aerosol optical depth from AERONET, J. Geophys. Res.-Atmos., 106, 12067–12097, doi:10.1029/2001jd900014, 2001.

Huang, J. P., Liu, J. J., Chen, B., and Nasiri, S. L.: Detection of anthropogenic dust using CALIPSO lidar measurements, Atmos. Chem. Phys., 15, 11653–11665, doi:10.5194/acp-15-11653-2015, 2015a.

Huang, J. P., Yu, H. P., Guan, X. D., Wang, G. Y., and Guo, R. X.: Accelerated dryland expansion under climate change. Nat. Clim. Change, 6, 166–172, doi:10.1038/nclimate2837, 2015b.

Huang, J. P., Minnis, P., Chen, B., Huang, Z. W., Liu, Z. Y., Zhao, Q. Y., Yi, Y. H., and Ayers, J. K.: Long-range transport and vertical structure of Asian dust from CALIPSO and surface measurements during PACDEX, J. Geophys. Res.-Atmos., 113, D23212, doi:10.1029/2008jd010620, 2008.

Huang, J. P., Minnis, P., Yan, H., Yi, Y., Chen, B., Zhang, L., and Ayers, J. K.: Dust aerosol effect on semi-arid climate over Northwest China detected from A-Train satellite measurements, Atmos. Chem. Phys., 10, 6863–6872, doi:10.5194/acp-10-6863-2010, 2010.

Huang, J. P., Wang, T. H., Wang, W. C., Li, Z. Q., and Yan, H. R.: Climate effects of dust aerosols over East Asian arid and semiarid regions, J. Geophys. Res.-Atmos., 119, 11398–11416, doi:10.1002/2014jd021796, 2014.

Jacob, D. J., Crawford, J. H., Kleb, M. M., Connors, V. S., Bendura, R. J., Raper, J. L., Sachse, G. W., Gille, J. C., Emmons, L., and Heald, C. L.: Transport and Chemical Evolution over the Pacific (TRACE-P) aircraft mission: Design, execution, and first results, J. Geophys. Res.-Atmos, 108, 1–19, doi:10.1029/2002jd003276, 2003.

Kim, W., Doh, S. J., and Yu, Y.: Anthropogenic contribution of magnetic particulates in urban roadside dust, Atmos. Environ., 43, 3137–3144, doi:10.1016/j.atmosenv.2009.02.056, 2009.

Laing, J. R., Jaffe, D. A., and Hee, J. R.: Physical and optical properties of aged biomass burning aerosol from wildfires in Siberia and the Western USA at the Mt. Bachelor Observatory, Atmos. Chem. Phys., 16, 15185–15197, doi:10.5194/acp-16-15185-2016, 2016.

Li, C., Tsay, S.-C., Fu, J. S., Dickerson, R. R., Ji, Q., Bell, S. W., Gao, Y., Zhang, W., Huang, J., Li, Z., and Chen, H.: Anthropogenic air pollution observed near dust source regions in northwestern China during springtime 2008, J. Geophys. Res.-

Atmos., 115, doi:10.1029/2009jd013659, 2010.
Li, G. J., Chen, J., Ji, J. F., Yang, J. D., and Conway, T. M.: Natural and anthropogenic sources of East Asian dust, Geology, 37, 727–730, doi:0.1130/g30031a.1, 2009.
Li, J., Wang, Z. F., Zhuang, G., Luo, G., Sun, Y., and Wang, Q.: Mixing of Asian mineral dust with anthropogenic pollutants over East Asia: a model case study of a super-duststorm in March 2010, Atmos. Chem. Phys., 12, 7591–7607, doi:10.5194/acp-12-7591-2012, 2012.Li, Z. Q., Lau, W. K. M., Ramanathan, V., Wu, G., Ding, Y., Manoj, M. G., Liu, J., Qian, Y., Li, J., Zhou, T., Fan, J., Rosenfeld, D., Ming, Y., Wang, Y., Huang, J., Wang, B., Xu, X., Lee, S. S., Cribb, M., Zhang, F., Yang, X., Zhao, C., Takemura, T., Wang, K., Xia, X., Yin, Y., Zhang, H., Guo, J., Zhai, P. M., Sugimoto, N., Babu, S. S., and Brasseur, G. P.: Aerosol and monsoon climate interactions over Asia, Rev. Geophys., 54, 866–929, doi:10.1002/2015rg000500, 2016.
Liu, Y., Sato, Y., Jia, R., Xie, Y., Huang, J., and Nakajima, T.: Modeling study on the transport of summer dust and anthropogenic aerosols over the Tibetan Plateau, Atmos. Chem. Phys., 15, 12581–12594, doi:10.5194/acp-15-12581-2015, 2015.
Mahowald, N. M. and Luo, C.: A less dusty future?, Geophys. Res. Lett., 30, 1903, doi:1910.1029/2003grl017880, 2003.
Mätzler, C.: MATLAB functions for Mie scattering and absorption, Res. Rep. 2002–08, Inst. Fur Angew. Phys., Bern, 2002.
McConnell, C. L., Formenti, P., Highwood, E. J., and Harrison, M. A. J.: Using aircraft measurements to determine the refractive index of Saharan dust during the DODO Experiments, Atmos. Chem. Phys., 10, 3081–3098, doi:10.5194/acp-10-3081-2010, 2010.
Mie, G.: Beiträge zur optic trüber Medien speziell kolloidaler Metallösungen, Ann. Phys., 25, 377–445, 1908.
Mishchenko, M. I., Lacis, A. A., Carlson, B. E., and Travis, L. D.: Nonsphericity of Dust-Like Tropospheric Aerosols – Implications for Aerosol Remote-Sensing and Climate Modeling, Geophys. Res. Lett., 22, 1077–1080, doi:10.1029/95gl00798, 1995.
Müller, T., Henzing, J. S., de Leeuw, G., Wiedensohler, A., Alastuey, A., Angelov, H., Bizjak, M., Collaud Coen, M., Engström, J. E., Gruening, C., Hillamo, R., Hoffer, A., Imre, K., Ivanow, P., Jennings, G., Sun, J. Y., Kalivitis, N., Karlsson, H., Komppula, M., Laj, P., Li, S. M., Lunder, C., Marinoni, A., Martins dos Santos, S., Moerman, M., Nowak, A., Ogren, J. A., Petzold, A., Pichon, J. M., Rodriquez, S., Sharma, S., Sheridan, P. J., Teinilä, K., Tuch, T., Viana, M., Virkkula, A., Weingartner, E., Wilhelm, R., and Wang, Y. Q.: Characterization and intercomparison of aerosol absorption photometers: result of two intercomparison workshops, Atmos. Meas. Tech., 4, 245–268, doi:10.5194/amt-4-245-2011, 2011.
Müller, T., Schladitz, A., Massling, A., Kaaden, N., Kandler, K., and Wiedensohler, A.: Spectral absorption coefficients and imaginary parts of refractive indices of Saharan dust during SAMUM-1, Tellus B, 61, 79–95, doi:10.1111/j.1600-0889.2008.00399.x, 2009.
Nakajima, T., Sekiguchi, M., Takemura, T., Uno, I., Higurashi, A., Kim, D., Sohn, B.

J., Oh, S. N., Nakajima, T. Y., Ohta, S., Okada, I., Takamura, T., and Kawamoto, K.: Significance of direct and indirect radiative forcings of aerosols in the East China Sea region, J. Geophys. Res.-Atmos, 108, 16, doi:10.1029/2002jd003261, 2003.

Nie, W., Ding, A. J., Wang, T., Kerminen, V. M., George, C., Xue, L. K., Wang, W. X., Zhang, Q. Z., Petaja, T., Qi, X. M., Gao, X. M., Wang, X. F., Yang, X. Q., Fu, C. B., and Kulmala, M.: Polluted dust promotes new particle formation and growth, Sci. Rep., 4, 6634, doi:10.1038/srep06634, 2014.

Park, S. U., and Park, M. S.: Aerosol size distributions observed at Naiman in the Asian dust source region of Inner Mongolia, Atmos. Environ., 82, 17–23, doi:10.1016/j.atmosenv.2013.09.054, 2014.

Patashnick, H. and Rupprecht, E. G.: Continuous PM-10 Measurements Using the Tapered Element Oscillating Microbalance, J. Air Waste Manage., 41, 1079–1083, doi:10.1080/10473289.1991.10466903, 1991.

Petzold, A., and Schönlinner, M.: Multi-angle absorption photometry—a new method for the measurement of aerosol light absorption and atmospheric black carbon, J. Aerosol Sci., 35, 421–441, doi:10.1016/j.jaerosci.2003.09.005, 2004.

Petzold, A., Kramer, H., and Schonlinner, M.: Continuous measurement of atmospheric black carbon using a multi-angle absorption photometer, Environ. Sci. Pollut. R., 78–82, 2002.

Prospero, J. M., Ginoux, P., Torres, O., Nicholson, S. E., and Gill, T. E.: Environmental characterization of global sources of atmospheric soil dust identified with the Nimbus 7 Total Ozone Mapping Spectrometer (TOMS) absorbing aerosol product, Rev. Geophys., 40, 1002 , doi:10.1029/2000rg000095, 2002.

Pu, W., Wang, X., Zhang, X. Y., Ren, Y., Shi, J. S., Bi, J. R., and Zhang, B. D.: Size Distribution and Optical Properties of Particulate Matter (PM10) and Black Carbon (BC) during Dust Storms and Local Air Pollution Events across a Loess Plateau Site, Aerosol Air Qual. Res., 15, 2212–2224, doi:10.4209/aaqr.2015.02.0109, 2015.

Qian, W. H., Tang, X., and Quan, L. S.: Regional characteristics of dust storms in China, Atmos. Environ., 38, 4895–4907, doi:10.1016/j.atmosenv.2004.05.038, 2004.

Ramanathan, V., Crutzen, P. J., Kiehl, J. T., and Rosenfeld, D.: Atmosphere - Aerosols, climate, and the hydrological cycle, Science, 294, 2119–2124, doi:10.1126/science.1064034, 2001.

Ramanathan, V., Ramana, M. V., Roberts, G., Kim, D., Corrigan, C., Chung, C., and Winker, D.: Warming trends in Asia amplified by brown cloud solar absorption, Nature, 448, 575–578, doi:10.1038/nature06019, 2007.

Rosenfeld, D., Clavner, M., and Nirel, R.: Pollution and dust aerosols modulating tropical cyclones intensities, Atmos. Res., 102, 66–76, doi:10.1016/j.atmosres.2011.06.006, 2011.

Schwarz, J.P., Gao, R.S., Spackman, J.R., Watts, L.A. and Thomson, D.S.: Measurement of the Mixing State, Mass, and Optical Size of Individual Black Carbon Particles in Urban and Biomass Burning Emissions, Geophys. Res. Lett., 35, 13810–13814, doi:10.1029/2008gl033968, 2008.

Rosenfeld, D., Rudich, Y., and Lahav, R.: Desert dust suppressing precipitation: A possible desertification feedback loop, Proc. Natl. Acad. Sci., 98, 5975–5980, doi:10.1073/pnas.101122798, 2001.

Seinfeld, J. H. and Pandis, S. N.: Atmospheric Chemistry and Physics, John Wiley and Sons, Inc., 2003.

Shi J. S., Tian P. F., Zhou T., and Huang Z. W.: Aerosol optical properties in spring in Agricultural area in Hexi Corridor, J. Arid Meteo., 33, 38–44, doi:10.11755/j.issn.1006-7639(2015)-01-0038, 2015 (in Chinese).

Shi J. S., Zhao M. G., Ge J. M., Bi J. R., Wang X., and Chen M.: The calibration of three-wavelength integration nephelometer, China Environ. Sci., 33, 1372–1378, 2013 (in Chinese).

Sloane, C. S., Rood, M. J., and Rogers, C. F.: Measurements of Aerosol-Particle Size - Improved Precision by Simultaneous Use of Optical-Particle Counter and Nephelometer, Aerosol Sci. Tech., 14, 289–301, doi:10.1080/02786829108959491, 1991.

Spracklen, D. V., and Rap, A.: Natural aerosol-climate feedbacks suppressed by anthropogenic aerosol, Geophys. Res. Lett., 40, 5316–5319, doi:10.1002/2013gl057966, 2013.

Srivastava, K. and Bhardwaj, R.: Analysis and very short range forecast of cyclone “AILA” with radar data assimilation with rapid intermittent cycle using ARPS 3DVAR and cloud analysis techniques, Meteorol. Atmos. Phys., 124, 97–111, doi:10.1007/s00703-014-0307-7, 2014.

Tao, J., Zhang, L., Cao, J., and Zhang, R.: A review of current knowledge concerning PM2. 5 chemical composition, aerosol optical properties and their relationships across China, Atmos. Chem. Phys., 17, 9485-9518, https://doi.org/10.5194/acp-17-9485-2017, 2017.

Tao, J., Zhang, L., Gao, J., Wang, H., Chai, F., and Wang, S.: Aerosol chemical composition and light scattering during a winter season in Beijing, Atmos. Environ., 110, 36-44, 2015.

Tao, J., Zhang, L., Ho, K., Zhang, R., Lin, Z., Zhang, Z., Lin, M., Cao, J., Liu, S., and Wang, G.: Impact of PM2.5 chemical compositions on aerosol light scattering in Guangzhou - the largest megacity in South China, Atmos. Res., 135–136, 48–58, 2014.

Tegen, I., and Fung, I.: Contribution to the Atmospheric Mineral Aerosol Load from Land-Surface Modification, J. Geophys. Res.-Atmos., 100, 18707–18726, doi:10.1029/95jd02051, 1995.

Tegen, I., Harrison, S. P., Kohfeld, K. E., Engelstaedter, S., and Werner, M.: Emission of soil dust aerosol: Anthropogenic contribution and future changes, Geochim. Cosmochim. Ac., 66, A766, 2002.

Tegen, I., Werner, M., Harrison, S. P., and Kohfeld, K. E.: Relative importance of climate and land use in determining present and future global soil dust emission. Geophys. Res. Lett., 31, L05105, doi:10.1029/2003gl019216, 2004.

Thompson, L. G., Davis, M. E., Mosleythompson, E., and Liu, K. B.: Pre-Incan Agricultural Activity Recorded in Dust Layers in 2 Tropical Ice Cores, Nature, 336, 763–765, doi:10.1038/336763a0, 1988.

Wang, S. G., Wang, J. Y., Zhou, Z. J., and Shang, K. Z.: Regional characteristics of three kinds of dust storm events in China, Atmos. Environ., 39, 509–520, doi:10.1016/j.atmosenv.2004.09.033, 2005.

Wang, X., Huang, J., Ji, M., and Higuchi, K.: Variability of East Asia dust events and their long-term trend, Atmos. Environ., 42, 3156–3165, doi:10.1016/j.atmosenv.2007.07.046, 2008.

Wang, X., Huang, J. P., Zhang, R. D., Chen, B., and Bi, J. R.: Surface measurements of aerosol properties over northwest China during ARM China 2008 deployment, J. Geophys. Res.-Atmos., 115, doi:10.1029/2009jd013467, 2010.

Wang, X., Pu, W., Shi, J., Bi, J., Zhou, T., Zhang, X., and Ren, Y.: A comparison of the physical and optical properties of anthropogenic air pollutants and mineral dust over Northwest China, J. Meteorol. Res., 29, 180–200, doi:10.1007/s13351-015-4092-0, 2015a.

Wang, X., Pu, W., Zhang, X., Ren, Y., and Huang, J.: Water-soluble ions and trace elements in surface snow and their potential source regions across northeastern China, Atmos. Environ., 114, 57–65, doi:10.1016/j.atmosenv.2015.05.012, 2015b.

Xin, J. Y., Du, W. P., Wang, Y. S., Gao, Q. X., Li, Z. Q., and Wang, M. X.: Aerosol Optical Properties Affected by a Strong Dust Storm over Central and Northern China, Adv. Atmos. Sci., 27, 562–574, doi:10.1007/s00376-009-9023-5, 2010.

Xin, J. Y., Wang, S. G., Wang, Y. S., Yuan, J. Y., Zhang, W. Y., and Sun, Y.: Optical properties and size distribution of dust aerosols over the Tengger Desert in Northern China, Atmos. Environ., 39, 5971–5978, doi:10.1016/j.atmonsenv.2005.06.027, 2005.

Xin, J. Y., Wang, Y. S., Pan, Y. P., Ji, D. S., Liu, Z. R., Wen, T. X., Wang, Y. H., Li, X. R., Sun, Y., Sun, J., Wang, P. C., Wang, G. H., Wang, X. M., Cong, Z. Y., Song, T., Hu, B., Wang, L. L., Tang, G. Q., Gao, W. K., Guo, Y. H., Miao, H. Y., Tian, S. L., and Wang, L.: The Campaign on Atmospheric Aerosol Research Network of China Care-China, B. Am. Meteorol. Soc., 96, 1137–1155, doi:10.1175/BAMS-D-14-00039.1, 2015.

Xu, J., Bergin, M. H., Greenwald, R., Schauer, J. J., Shafer, M. M., Jaffrezo, J. L., and Aymoz, G.: Aerosol chemical, physical, and radiative characteristics near a desert source region of northwest China during ACE–Asia, J. Geophys. Res., 109, D19S03, doi:10.1029/2003jd004239, 2004

Yan, H.: Aerosol scattering properties in northern China, Atmos. Environ., 41, 6916–6922, doi:10.1016/j.atmosenv.2007.04.052, 2007.

Yang, M., Howell, S. G., Zhuang, J., and Huebert, B. J.: Attribution of aerosol light absorption to black carbon, brown carbon, and dust in China – interpretations of atmospheric measurements during EAST-AIRE, Atmos. Chem. Phys., 9, 2035–2050, doi:10.5194/acp-9-2035-2009, 2009.

Zhang, X. Y., Arimoto, R., and An, Z. S.: Dust emission from Chinese desert sources linked to variations in atmospheric circulation, J. Geophys. Res.-Atmos., 102,

28041–28047, doi:10.1029/97jd02300, 1997.
Zhang, X. Y., Wang, L., Wang, W. H., Cao, D. J., Wang, X., and Ye, D. X.: Long-term trend and spatiotemporal variations of haze over China by satellite observations from 1979 to 2013, Atmos. Environ., 119, 362–373, doi:10.1016/j.atmosenv.2015.08.053, 2015.
Zhang, X. Y., Wang, Y. Q., Wang, D., Gong, S. L., Arimoto, R., Mao, L. J., and Li, J.: Characterization and sources of regional-scale transported carbonaceous and dust aerosols from different pathways in coastal and sandy land areas of China, J. Geophys. Res.-Atmos., 110, D15301, doi:10.1029/2004jd005457, 2005.